XMM-Newton

XMM-Newton Science Analysis System versions 13.0 & 13.5 - scientific validation report

XMM-SOC-USR-TN-0023 Issue 1.1

C.Gabriel, E. Chapin, I. de la Calle, A.Ibarra, R.González-Riestra, M.Guainazzi, A.L.Longinotti, E.Ojero, A.Pollock, P. Rodríguez, R.Saxton, M. Smith, M.Stuhlinger, A.Talavera
XMM-Newton Science Operations Centre

28 February 2014

Revision history

Revision number	Date	Revision author	Comments
0.9	18 February 2013	C. Gabriel	Plan SAS 13.0 including schedule
0.95	22 October 2013	C. Gabriel	Plan SAS 13.5 including schedule
1.0	18 February 2014	C. Gabriel et al	All inputs merged - Full report
1.1	28 February 2014	C. Gabriel	Wrong tables for `multixmmselect` tests replaced

Contents

1 Introduction

1.1 Concept

Scientific Validation (SV) is required in order to ensure a constant high quality of the XMM-Newton Science Analysis System (SAS). This document has the particularity of addressing the two validation processes for SAS 13.0 and SAS 13.5 taking place during 2013.
The main purpose of the SV is to provide the SAS community with a stable reliable software product, as well as to generate a list of caveats and known deficiencies. Together with these "functional" tests, the SV provides some information on the expected systematic uncertainties when basic data analysis products are generated through the current version of the SAS, using the best calibrations available at the moment SAS was released. It is important to stress that *this document does not supersede or substitute* the **instrument calibration status documents**, available from the XMM-Newton calibration portal. Instrument calibration is a continuous activity, whose results (update of calibration files) is intrinsically and necessarily decoupled from software releases. XMM-Newton users are recommended to consult periodically the URL: `http://xmm.esac.esa.int/external/xmm_sw_cal/calib`, which informs on the calibration status of the XMM-Newton instruments.
The SV is performed on a standard set of XMM-Newton observations, which cover all commissioned observational modes, and a number of observations, specially chosen for testing new / special aspects of the data reduction corresponding to the version to be validated. Tab. 1 lists all the datasets used for the validation of SAS versions 13.0 and 13.5. Some of these observations are particularly suitable to test calibration-related items, as specified in the rightmost column of Tab. 1. These datasets are partly intended as a standard reference, which has been and will be used to verify the performances of all SAS versions. However, additional datasets may occasionally be used to test version-specific SAS items. This is the case, for instance, for the datasets discussed in Sect. 3 of this report. Datasets discussed in a given report and not listed in Tab. 1 do not belong to the reference datasets, and are therefore not intended to be discussed in later SAS versions validation reports.

1.2 Methodology

The SV for SAS v13.0 and SAS v13.5 consists of the following steps:

1. all the datasets listed in Tab. 1 are processed through the SAS 13 based testing Pipeline System (PPS) running at the SOC, and

2. the same datasets are also processed through the SAS reduction meta-tasks: `e[mp]proc`, `om[ifg]chain`, `rgsproc`

3. products generated by the above steps are used as basis for the *interactive SV analysis*. Standard scientific products (images, light curves, spectra, source lists) are generated and analyzed. This allows to:

   - test the SAS interactive tasks.
   - verify the calibration accuracy obtained, and compare it with the expected accuracy on the basis of the calibration status at the time the SV is performed.

4. in addition the whole cross-calibration database is reduced by standard analysis scripts based on SAS but including also model fitting through Xspec.

Table 1: SV datasets

Instrument	Mode	Object	Revolution Obs. ID	ID	Calibration item
EPIC MOS	Full Frame	Lockman Hole	544 0147511601	1	Astrometry + source detection
	”	G21.5.09	060 0122700101	2	Effective area
	Small Window (W2)	Mkn 421	165 0099280201	3	
	Large Window (W3)	PKS0558-504	153 0129360201	4	Effective area
	Timing Uncompressed	Her X-1	207 0134120101	5	Timing
EPIC-pn	Full Frame	Lockman Hole	544 0147511601	1	Astrometry
	Full Frame/Small Window	PKS0558-504	153 0129360201	4	Effective area
	Large Window	AB Dor	185 0133120201	6	
	Small Window	PKS0558-504	084 0125110101	7	Effective area
	Fast Timing	Her X-1	207 0134120101	5	Timing
		Crab	698 0160960201	8	
	Fast Burst	Crab	411 0153750301	9	Timing
		Crab	411 0153750501	10	Timing
	Extended Full Frame	G21.5-0.9	060 0122700101	2	Effective area
	Slew Data		1388 9138800002	18	Slew data processing
	Slew Data		1450 9145000003	19	Slew data processing
RGS	SPEC+Q	PKS0558-504	084 0125110101	7	
”		Mkn 421	165 0099280201	3	Effective area
	”	AB Dor	185 0133120201	6	Wavelength scale
	”	AB Dor	338 0134521301	11	Wavelength scale
	”	AB Dor	462 0134521601	12	Wavelength scale
	”	AB Dor	572 0134522201	13	Wavelength scale
OM	Image Mode	BPM 16274	261 0125320701	14	Photometry
	Fast Mode	X1822-371	228 0111230101	15	
	FF Low Resolution	BPM 16274	261 0125320701	14	Astrometry
	Optical grism	Hz2	503 0125910901	16	Wavelength scale & flux calibration
	UV Grism	HD13499 (offset)	657 0125911301	17	Wavelength scale & flux calibration

5. and in the validation of SAS 13.5 all the threads offered in the SAS web pages (http://xmm.esac.esa.int/sas/current/documentation/threads/) have been used for data analysis. In this way we insure on the one side that more SAS tasks are tested under a fix configuration, and on the other side that the threads are fully valid for the new version. Several threads have been accordingly updated through this exercise.

The conclusions of the SV are summarized in Sect. 5.
It is to be noticed that by far not all the checks and comparisons performed during the scientific validation are reported here, but only those which are considered relevant with respect to the accuracy of the calibration or represent new achievements and / or corrections.
In this report: best-fit parameter uncertainties are at the 90% confidence level for 1 interesting parameter ($\Delta\chi^2 = 2.71$); errors on positions or count rates are at the 1-σ level; energies are quoted in the observer's reference frame unless otherwise specified.

2 New in SAS 13

There are several new elements as well as fundamental upgrades in SAS v13.0 with respect to former versions. They can consist of new tasks, or new analysis methods within already existing tasks. All of them have to be scientifically validated, in addition to their standard integration tests.

2.1 New in SAS13: Pile-up correction

A novel method (Added Event method) for correcting the effects of pile-up is introduced in SAS 13: it consists in adding trial events to the original event file and following their evolution to find what fraction are upscattered by pile-up and to what energies. The resultant channel spectrum is written into the RMF. The advantages of this method is that no previous assumption about the non piled-up spectrum have to be made. It can be applied only to PN data, however, due to the on-board discarding of anomalous events in the case of MOS.
Validation should be done on the basis of both real and simulated data. Cases for real data could be either a) non-variable sources observed both in full frame and small window mode, the latter being not piled-up or b) any piled-up source, allowing for a good comparison of the spectrum extracted from an annulus, and the corrected spectrum of the whole source.

2.2 Upgraded in SAS13: 2D PSF

There have been several upgrades in the 2D PSF approach, and the results of intensive testing related to the 3XMM catalogue derivation have shown that there is an off-axis dependent displacement of the centroid of the 2D PSF model applied compared to the true position of a source. This correction is implemented in SAS 13 as part of the 2D PSF CAL derivation, while for the 3XMM catalogue it was applied by a final external correction. The EPIC data used for astrometry (Lockman Hole observation 0147511601 in revolution 544) should be analysed in terms of sources found using the upgraded "2D PSF" and compared to the results in the 3XMM catalogue.

2.3 New in SAS13: X-Ray Loading correction for EPIC-pn imaging modes

X-ray loading (XRL) corrections should be applied also to PN imaging modes. A new task (`epxrlcorr`) dealing with it produces XRL maps, shifting correspondingly the PHA energies of the input ODF PN data.
Testing will be defined by the EPIC Instrument Dedicated Team.

2.4 New in SAS13: EPIC overlapping data treatment

More and more sky fields have been repeatedly observed in the XMM-Newton lifetime, also the mosaic observation mode is increasingly used, with more or less overlapping area. Every time XMM-Newton observes a field, three different cameras are obtaining data. All these facts together contribute to the desire of processing this kind of data at once, instead of exposure by exposure, and also to combine the spectral data. An extension of the `xmmselect` capabilities, making it able to handle any number of exposures at the same time is provided with SAS 13. Selection of source and background region in a combined image is therefore possible, followed by an eventual optimization and extraction of source and background spectra from everyone of the input exposures. Combined source and background spectra can be obtained, together with a corresponding response matrix, for easing the handling.
Multiple observations, if possible in different observing modes, of the same area should be used for testing.

2.5 New in SAS13: RGS solar aspect angle dependency and heliocentric corrections

A wavelength scale dependency of the RGS spectrometers from the solar aspect angle at the time of an observation has been established, which SAS 13 will correct for. In addition, heliocentric corrections will be applied also modifying the spectrum (in SAS 12 the derivation of the heliocentric value and its inclusion as a keyword header for further use in spectral fitting had been introduced). The quality of the corrections should be measured by a reduction of the systematic uncertainties related to the wavelength scale.
All the 4 different AB Dor observations contained in the standard data set should be used for this purpose.

2.6 Upgraded in SAS13: OM S/W

Although not fundamental changes have been applied in this version to the specific OM S/W a number of upgrades have taken place.
It follows the list of changes applied to the SAS OM S/W in SAS 13:

- astrometry correction in `omatt`: a call to wcstools has been introduced to create a subset of the USNO catalog to be used in the optional cross correlation. If the user has provided that file, then this new feature is not used.
- search for variability in `omichain`: `omvariability` has been included in `omichain`, so that in case of multiple exposures with the same filter this task is run to detect variable sources.
- deeper source detection: in case of mosaiced or stacked images, `omichain` runs `omdetect` on the mosaiced/stacked image to detect faint sources which were not

seen in the single image. This produces a new source list that is merged with the original one produced by `omsrclistcomb` (the detections made in the original raw images are maintained, only new detected sources are added to the combined list).

- ds9 region from the combined source list: this is a ds9 compatible region produced in RA/Dec to be used overlaid in the final sky aligned image. It is produced by `omregion` within `omichain`.
- detection limits: `omsrclistcomb` now adds keywords in the combined source list with the detection limits in the used filters.
- fast mode chain `omfchain`: the default background extraction has been changed to using the image mode background. This is a better approach in general.
- a set of utilities called `omcat` have been introduced in SAS 13. These tasks are intended only for usage by the SOC in the generation of OM catalogs.

3 New in SAS 13.5

SAS 13.5 is an intermediate version, which is going to be released due to the importance of its main upgrade, the calibration of the temporal response variation of the MOS cameras based on a contamination model. This calibration is contained both in new S/W and new calibration files. Another important item is the rate dependent correction of the PN Timing mode. Several OM SAS tasks have also been upgraded as part of the preparation for the next OM catalogue release.

3.1 New in SAS13.5: EPIC-MOS contamination correction

The deterioration of the response of the MOS cameras (especially MOS2) at low energies ($\leq 1keV$) over the course of the mission can be modeled as due to contaminants adhered to the surface of the cameras, absorbing a fraction of the incoming photons. With the help of a new calibration file (EMOS[1-2]_CONTAMINATION) the time dependency of the response is partly satisfactorily reproduced as the product of a pure Carbon layer lying on the cameras, similar to what has been observed with the RGS cameras.
Validation should be done on the basis of real data, covering all the different epochs since the beginning of the XMM-Newton mission. The EPIC IDT will lead a validation campaign for this correction, given the strong implications and the change of paradigm for the temporary response evolution. The X-Cal data offers an ideal set for this validation.

3.2 Upgraded in SAS13.5: EPIC-pn Timing Mode calibration refinement

The energy scale in EPIC-PN Timing Mode can now be corrected either by the rate dependant PHA correction (RDPHA, parameter "withrdpha" in epevents, introduced in SAS 13) or by the rate dependent CTI correction (RDCTI, (applied through the standalone SAS task epfast). Both corrections are mutually exclusive. Validation should not only establish the level of accuracy reached through these corrections, but also make sure that under no circumstances the data is overcorrected (by applying consecutively both corrections). A set of 84 exposures in this observing mode has been identified by the EPIC Calibration Scientist for performing the validation. It will be annexed to the Calibration Status document.

4 Results of the validation exercises

4.1 SAS 13.0 validation

The standard validation has proceeded as planned, with the reduction of all the standard datasets via scripts based on `epicproc / rgsproc / om[i,g,f]chain`. Data was nominally reduced as well as with a test version of the pipeline based on SAS 13. Also the XCal archive has been fully processed with SAS 13, the cross-calibration results have been taken for an upgrade of the Calibration Document. Screening of PPS processed standard datasets has been performed as the interactive analysis and the new / updated features dedicated analysis were. SAS 13 was finally released on May 6.
There were no errors in any of the reductions, neither with the "procs" nor with the SAS 13.0 based pipeline. The results from the cross-calibration exercise are considered globally fully acceptable and can be consulted through the Cross Calibration Review tool (http://xmm2.esac.esa.int/cgi-bin/ept/preview.pl).

4.1.1 G21.5 analysis

In SASv11 and earlier the mask description in the header of the instrument mask files produced by `emask` was wrong. This prevented `arfgen` from calculating the correct effective area when a mask was used to select good events for the accumulation of scientific products. Here we report for the first time the results of the application of the corresponding software bug fix to the spectral analysis of an early observation of the non-thermal SNR G21.5-0.9. This observation has been used for the scientific validation EPIC cameras spectral analysis reproducibility since the first SAS Science Validation Report (Gabriel et al. 2002).
Data reduction and spectral analysis followed the procedure as described in, *e.g.* Gabriel at al. 2008. Spectra and associated responses were extracted from a common region in the sky defined by `AND`-merging the instrument masks of the three EPIC cameras. The results are summarised in Fig. 1. They are in excellent agreement with those published in Tsujimoto et al. 2011, where a preliminary implementation of the software fix in a SAS development (*i.e.* non public) version was employed (please, be aware that fluxes 2–8 keV energy band are reported in the Tsujimoto et al. paper).

4.1.2 Pile-up correction

The functional validation of the new correction implemented in SAS 13 (Added Event method) has been successful performed using several PN datasets. A qualitative impression can be gathered through Figs. 2 and 3. In the first one, a heavily piled-up observation of Markarian 421 (Obs. ID 0136540701) is fitted before and after the correction with a single power-law model. The red line is the fit after the correction. The slope changes from $\Gamma = 1.94$ to $\Gamma = 2.19$ and the flux in the range $E = [0.2 - 10]keV$ gets increased from F = 4.8x10^{-10} erg cm^{-2} s^{-1} to F = 14.1x10^{-10} erg cm^{-2} s^{-1}. The second one is a lightly piled-up observation of the same source, here the flux gets only increased by 3% and the slope varies from 2.51 to 2.54.
A full scientific validation, showing strengths and limits, is however out of the scope of this exercise and will need dedicated efforts. For the time being, and until this happens, the Pile-up correction is considered experimental.

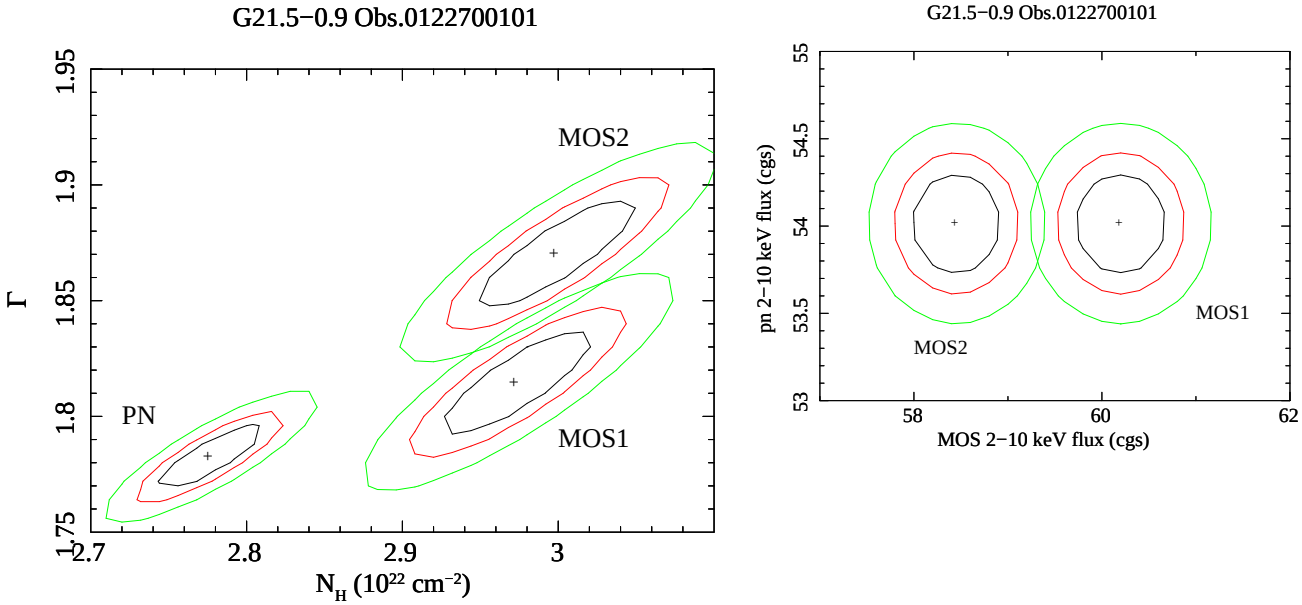

Figure 1: *Left panel*: iso-χ^2 contours for the column density versus the photon index when a simple photoelectrically absorbed power-law model is applied to the EPIC spectra of G21.5-0.9 in Obs.#0122700101. The contours indicate the 68%, 90% and 99% confidence levels for two interesting parameters. *Right panel*: the same for the 2–10 keV absorption corrected fluxes.

4.1.3 X-ray loading correction for imaging modes - `epxrlcorr`

In order to validate the X-ray loading (XRL) correction task `epxrlcorr` two PN imaging mode observations showing clear signs of X-ray loading have been analysed:

- The Seyfert galaxy NGC 2992 was observed by XMM-Newton in an X-ray high state in May 2003 (ObsID 0147920301). EPIC-pn was operated in Full Frame mode, configured with the Medium filter. The time averaged source count rate in the pn is 20 cs^{-1}, which is well above the pile-up (PU) threshold of 6 cs^{-1} for this mode. Moreover, the offset map taken at the beginning of the exposure reveals pixels with significant residual offsets within $\sim$ 8" radius of the source location, up to a maximum of 91 ADU in the PSF central pixel (see Fig. 4, left panel.). Given the source's weak optical emission (V_{mag} = 12.2), the residual offsets can be entirely ascribed to X-ray loading (XRL) at the PSF core. In fact, the residual offset values are fully consistent with being due to XRL for a point source at this count rate in Full Frame mode.

- The X-ray transient SAX J1711.6-3808 was observed in outburst with EPIC-pn in Full Frame mode with Thin filter in March 2001 (ObsID 0135520401). With a mean source count rate in pn of 56 cs^{-1} this source is subject to significant PU. There are very substantial residual offsets due to XRL reaching a maximum of 782 ADU at the centre of the PSF (see Fig. 4, right panel), consistent with the source count rate and spectral shape.

In addition to significant XRL, both sources are subject to substantial PU, the combined effects of which are shown in the respective pattern fraction plots in Fig. 5.
For data taken from circular regions of radius 100" at the source locations the pattern fractions show significant deviations from the nominal pattern fraction distribution. A relative excess of single events at lower energies, and a deficit of single events at higher energies, results from the

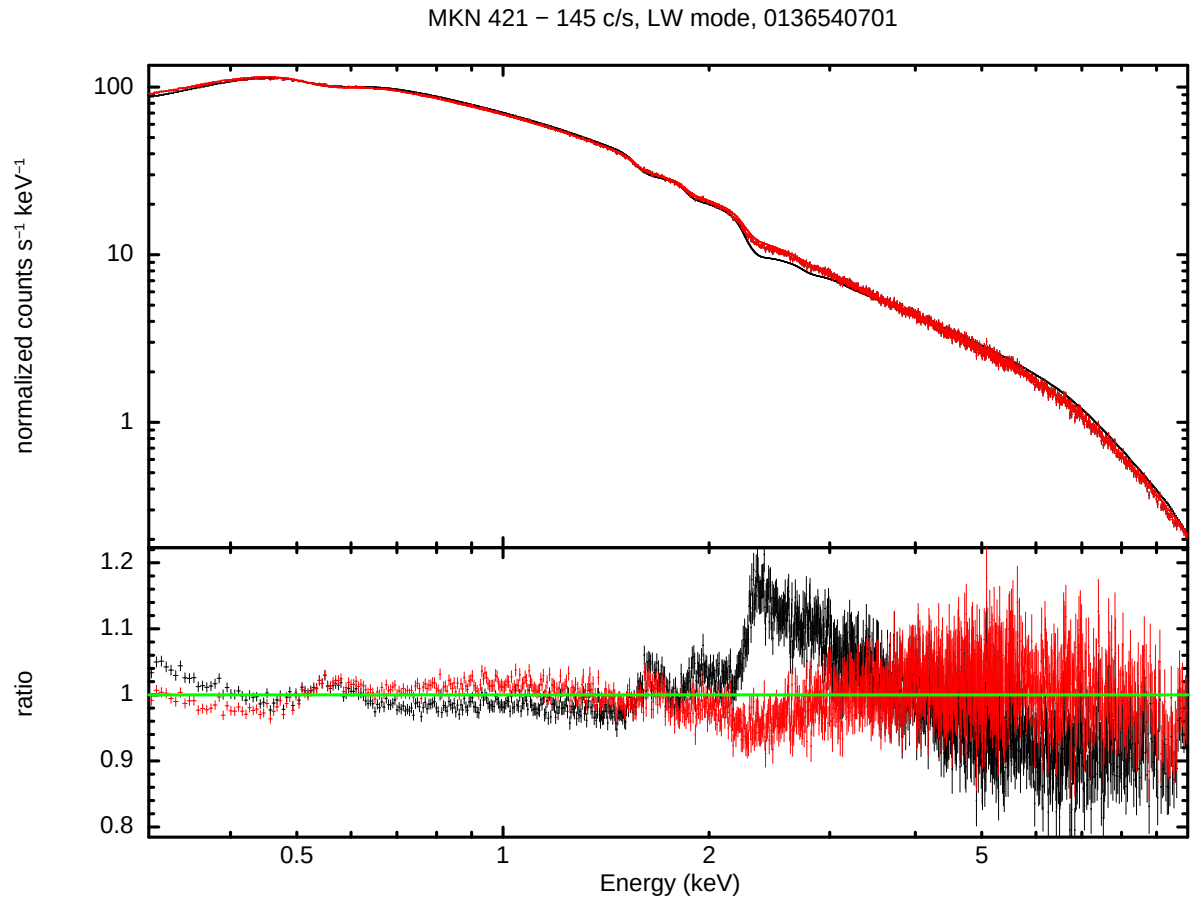

Figure 2: Fitted spectra of a heavily piled-up observation of Markarian 421, before (black) and after (red) pile-up correction. The model used is a simple power-law.

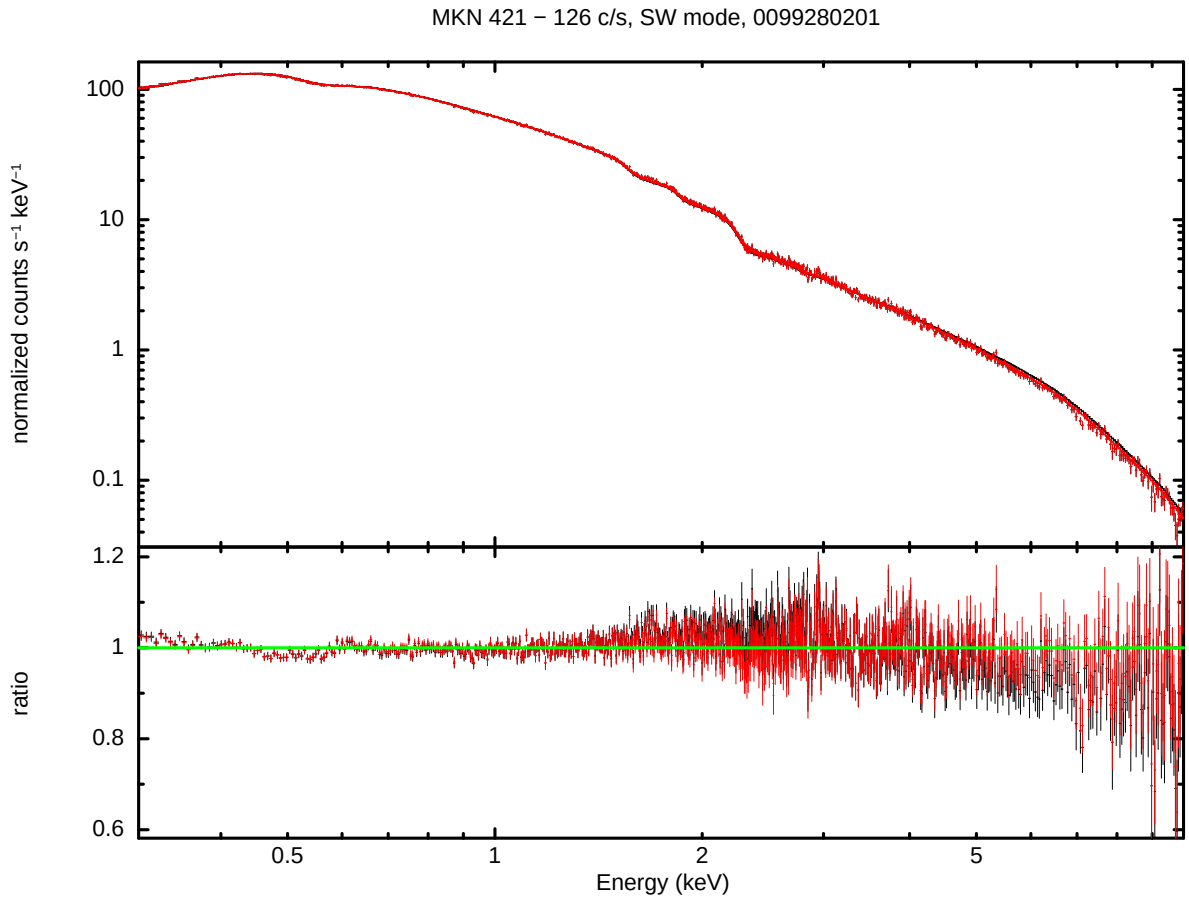

Figure 3: Fitted spectra of a lightly piled-up observation of Markarian 421, before (black) and after (red) pile-up correction. The model used is a simple power-law.

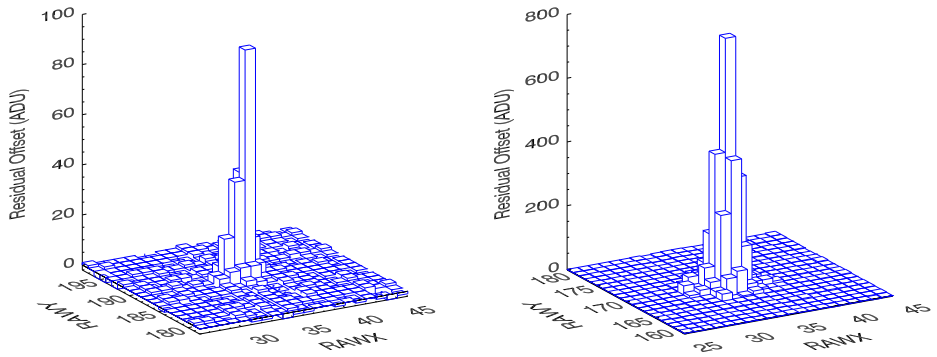

Figure 4: Residual offsets in ADU due to XRL of NGC 2992 (left) and SAX J1711.6-3808 (right). Only the chip areas around the source locations are shown.

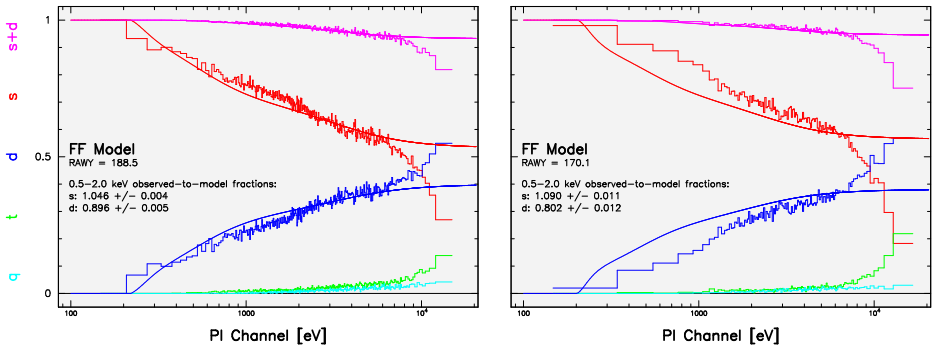

Figure 5: Pattern fraction distributions of circular source extraction regions showing combined effects of PU and XRL. Left: NGC 2992, right: SAX J1711.6-3808.

combined effects of PU and XRL. For a quantitative comparison of the SAS XRL correction, the corrected spectra should be compared with XRL-free spectra. The latter are obtained by avoiding data from a suitably large region at the PSF core, through an annular source extraction region. As this data will be free of both XRL and PU, correction for both these effects should be made in order to allow a proper comparison.
For NGC 2992, a qualitatively acceptable pattern distribution is obtained by excising the PSF core through an annular extraction region with inner radius of 10" whereas for SAX J1711.6-3808 the required core radius is 20".
It is assumed that the data extracted from the respective annular regions have a sufficiently low PU fraction and are also XRL free as the pixels with significant XRL have been excluded. Per target, a source spectrum was extracted from the PU and XRL free annular region, and was used to define the best fit model parameters for subsequent comparison with PU and XRL corrected data, which were extracted from a circular region. In each case, a background spectrum was obtained from a source-free region located at the same RAWY coordinate as the source.
XRL correction is performed by the `epxrlcorr` task, which adjusts each event energy according to the residual offset measured in the respective pixel. PU correction is performed by the task `rmfgen` by setting `correctforpileup=yes` and `raweventfile=events04.dat` (where `events04.dat` is an intermediate file created by `epchain`). The SAS version used in this analysis is `xmmsas_20130501_1901-13.0.0`, with task versions `epxrlcorr-0.1.6` and `rmfgen-2.0.5`.

NGC 2992

Spectral fitting of NGC 2992 in the $0.4 - 12.0$ keV band was performed with XSPEC using a model based on Shu et al. 2010, consisting of the following components: partial covering absorption (PARTCOV), disk emission around a Schwarzschild black hole (DISKLINE), optically thin thermal emission (APEC), Compton reflection (PEXRAV), and two unresolved Gaussian components for Fe Kα and Fe Kβ emission from distant matter. The best fit resulted in a χ^2 of 1833.7 for 1603 degrees of freedom. The spectrum and best fit model residuals are shown in Fig. 6 (top panel). For comparison, the figure also shows the spectrum obtained from the

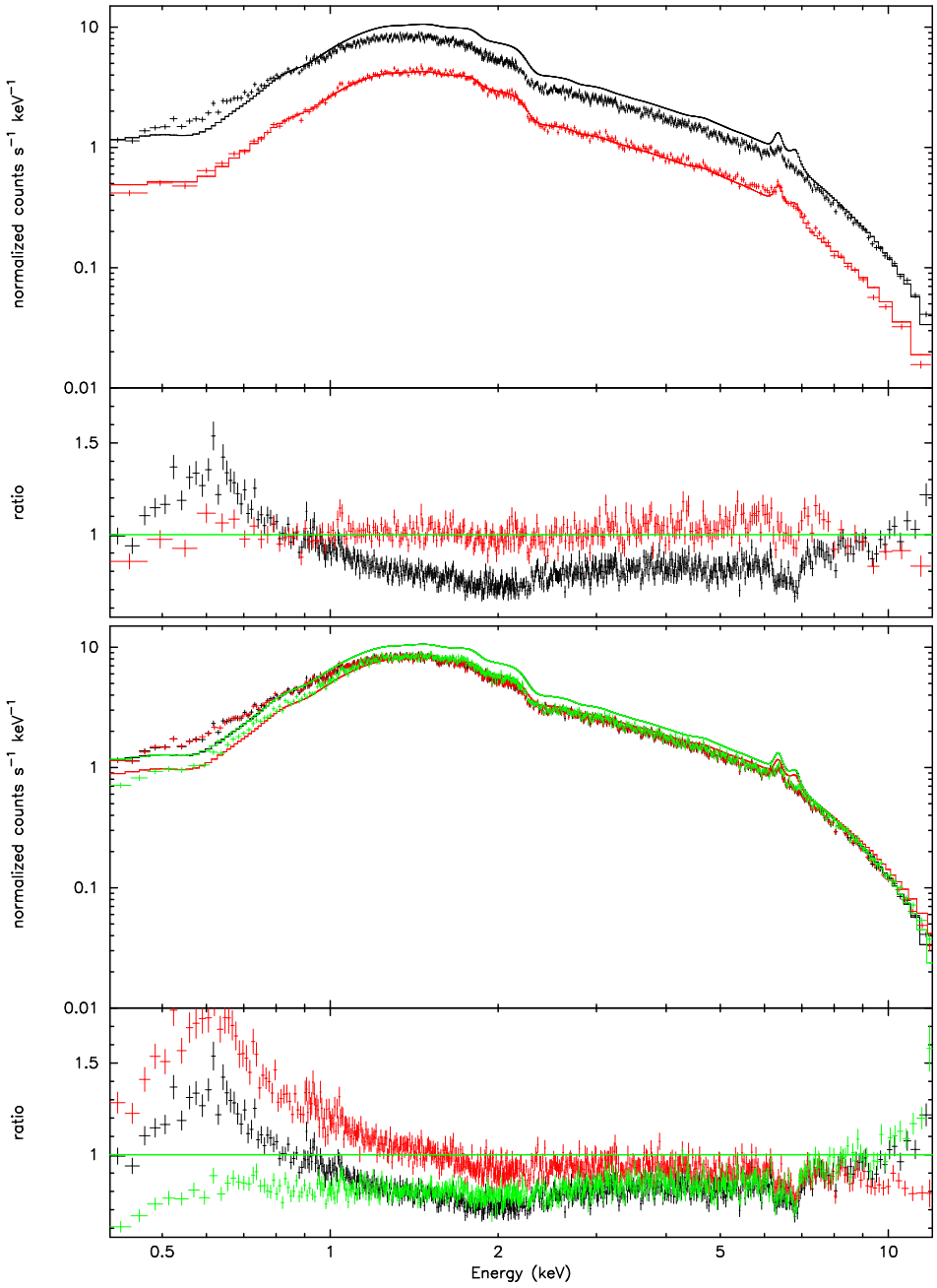

Figure 6: NGC 2992 spectra and data-to-model residuals. The model used is that obtained from the best fit to the annular region data (the data have been binned to a signal-to-noise ratio of 20 for clarity). *Top panel:* NGC 2992 spectra obtained from a circular (black) and annular (red) extraction region. The circular region spectrum is clearly distorted due to the combined effects of PU and XRL in the PSF core. *Bottom panel:* NGC 2992 spectra obtained from a circular extraction region: uncorrected (black), with PU correction only (red) and with XRL correction only (green).

circular extraction region, which is obviously distorted due to the effects of PU and XRL.

- PU correction only: Fig. 6 (bottom panel) shows the PU corrected spectrum in red, and the

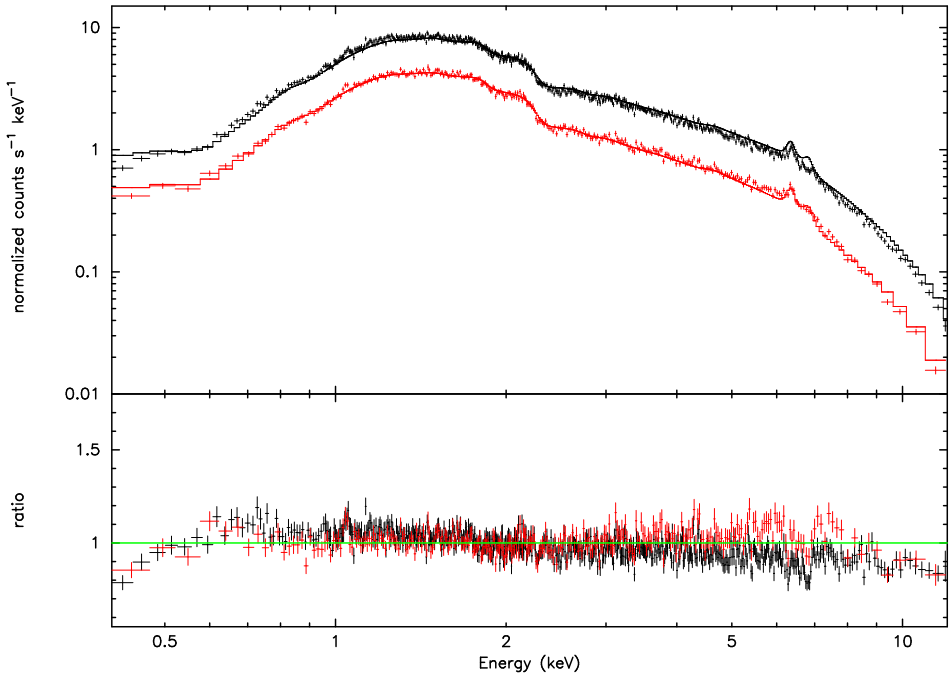

Figure 7: NGC 2992 spectra obtained from an annular region (red) and from a circular region (black), the latter having been corrected for both XRL and PU. As before, the model used is that obtained from the best fit to the annular region data.

uncorrected spectrum in black for comparison. The corrected data show some recuperation of the apparent flux loss due to PU, but the residuals show large discrepancies mainly due to a pixel dependent shift of the energy scale owing to the uncorrected XRL.

• XRL correction only: the bottom panel in Fig. 6 shows the XRL corrected data in green. The shifted event energies result in substantially flattened residuals with respect to those of the uncorrected data.

• Combined XRL and PU correction: Fig. 7 shows the spectrum after applying both XRL and PU corrections (in black). For comparison, the annular region spectrum (in red) and best-fit model are also shown. The corrected data show similar shaped residuals to the annular region spectrum, the main difference, however, being its steeper spectral slope. The best fit of the model to the corrected spectrum yields a χ^2 of 2130.6 for 1913 degrees of freedom. The results of the spectral fitting are summarised in Table 2. Most significantly, the corrected spectrum shows a higher photon index, by ~ 0.08, which could indicate a PU over-correction leading to a spectral softening.

SAX J1711.6-3808 SAX J1711.6-3808 was fit in the $0.7-12$ keV band with a model consisting of a power law with high energy exponential rolloff (CUTOFFPL), interstellar absorption (WABS)

and an emission line from an accretion disk around a black hole (LAOR) (in 't Zand et al. 2002, and Sánchez-Fernández et al. 2006). The best fit yielded a χ^2 of 1317.6 for 1320 degrees of freedom. The spectrum and best fit model residuals are shown in Fig. 8 (top panel). As before, the figure also includes the spectrum affected by PU and XRL obtained from the circular extraction region.

• PU correction only: Fig. 8 (bottom panel) shows the PU corrected spectrum in red, and the uncorrected spectrum in black for comparison. At the high level of PU present in this exposure the correction yields an insufficient recovery of the apparent flux loss. In addition, the residuals show large discrepancies due to the XRL-induced distortion of the energy scale.

• XRL correction only: the bottom panel in Fig. 8 shows the XRL corrected data in green. The corrected energy scale yields generally flattened residuals with respect to those of the uncorrected data.

• Combined XRL and PU correction: Fig. 9 shows the spectrum after applying both XRL and PU corrections (in black). For comparison, the annular region spectrum (in red) and best-fit model are also included. The residuals are dominated by the $\sim 50\%$ unrecovered flux due to insufficient PU correction. However, the XRL correction has resulted in a substantial reduction of the large residuals at lower and higher energies. In fact, a fit of the model to the corrected spectrum, yielding a χ^2 of 1848.2 for 1732 degrees of freedom (see Table 3) shows similar values for spectral slope and absorption. The most significant differences with respect to the model based on annular data are seen at energies above ~ 5 keV, and could be ascribed to the insufficient PU correction.

4.1.4 X-ray loading correction for fast modes - `epreject`

With SASv12, `epreject` supports the X-ray Loading Correction (Smith, 2004, XMM-CAL-TN-0050) for EPIC-pn Fast Modes (Burst and Timing). With SASv13 we have introduced the first calibration of this correction (see Guainazzi et al. 2012 for a description). The `epreject` implementation was validated by comparing PHA spectra extracted from Obs.#0410180101 when the constant term of the XRL correction was set to 0, and -6.9 (Guainazzi et al. 2012). As expected, the PHA distributions differ by -7.0. The small difference ($\simeq$0.1, corresponding to $\simeq$0.5 eV) between the expected and the measured value is due to a randomisation posterior to the XRL correction.

4.1.5 `eradial` - accuracy of the 2D PSF (ELLBETA)

In SASv13 `eradial` includes a more accurate algorithm to calculate the exact contribution of each pixel to the source radial profile. This algorithm was tested using an observation of the bright Active Galactic Nucleus MCG-6-30-15 (Obs.#0029740801). With the new algorithm, the nominal $\pm 2\%$ accuracy of the `ELLBETA` PSF calibration is recovered (Read et al. 2011; Fig. 10).

Table 2: Comparison of NGC 2992 best-fit spectral parameters for the data from an annular region and the XRL and PU corrected data respectively. Only the free parameters are shown here.

Model Component	Parameter	Value (annulus)	Value (corrected)
WABS	N_H (10^{21} cm^{-2})	$7.3^{+0.1}_{-0.1}$	$7.3^{+0.1}_{-0.1}$
PEXRAV	Γ	$1.796^{+0.013}_{-0.014}$	$1.878^{+0.011}_{-0.010}$
PEXRAV	I (10^{-3} ph keV^1 cm^{-2} s^{-1})	$30.4^{+0.5}_{-0.5}$	$31.9^{+0.4}_{-0.4}$
DISKLINE	R_{out} (GMc^{-2})	13^{+6}_{-3}	13^{+3}_{-3}
DISKLINE	θ (deg)	38^{+4}_{-2}	40^{+2}_{-2}
DISKLINE	I (10^{-5} ph cm^{-2} s^{-1})	34^{+5}_{-6}	20^{+4}_{-4}
ZGAUSS	E [Fe Kα] (keV)	$6.397^{+0.026}_{-0.022}$	$6.413^{+0.020}_{-0.016}$
ZGAUSS	$norm$ [Fe Kα] (10^{-5} ph cm^{-2} s^{-1})	11^{+2}_{-2}	9^{+1}_{-1}
χ^2/d.o.f.		1833.7/1603	2130.6/1913

Table 3: Comparison of SAXJ1711.6-3808 best-fit spectral parameters for the data from an annular region and the XRL and PU corrected data respectively. Only free parameters are shown.

Model Component	Parameter	Value (annulus)	Value (corrected)
WABS	N_H (10^{22} cm^{-2})	$2.30^{+0.09}_{-0.11}$	$2.03^{+0.05}_{-0.07}$
CUTOFFPL	Γ	$1.04^{+0.14}_{-0.15}$	$1.05^{+0.05}_{-0.11}$
CUTOFFPL	E_{cutoff} (keV)	$5.68^{+0.9}_{-0.8}$	$8.66^{+2.6}_{-2.5}$
CUTOFFPL	I (ph keV^1 cm^{-2} s^{-1})	$0.28^{+0.03}_{-0.03}$	$0.13^{+0.01}_{-0.01}$
LAOR	E (keV)	$6.3^{+0.1}_{-0.1}$	$6.3^{+0.1}_{-0.1}$
LAOR	R_{in} (GMc^{-2})	13^{+3}_{-2}	37^{+2}_{-1}
LAOR	θ (deg)	$86.2^{+0.3}_{-1.0}$	$87.0^{+2.0}_{-1.2}$
LAOR	$norm$ (10^{-3} ph cm^{-2} s^{-1})	$7.34^{+1.1}_{-1.0}$	$1.02^{+0.6}_{-0.4}$
χ^2/d.o.f.		1317.6/1320	1848.2/1732

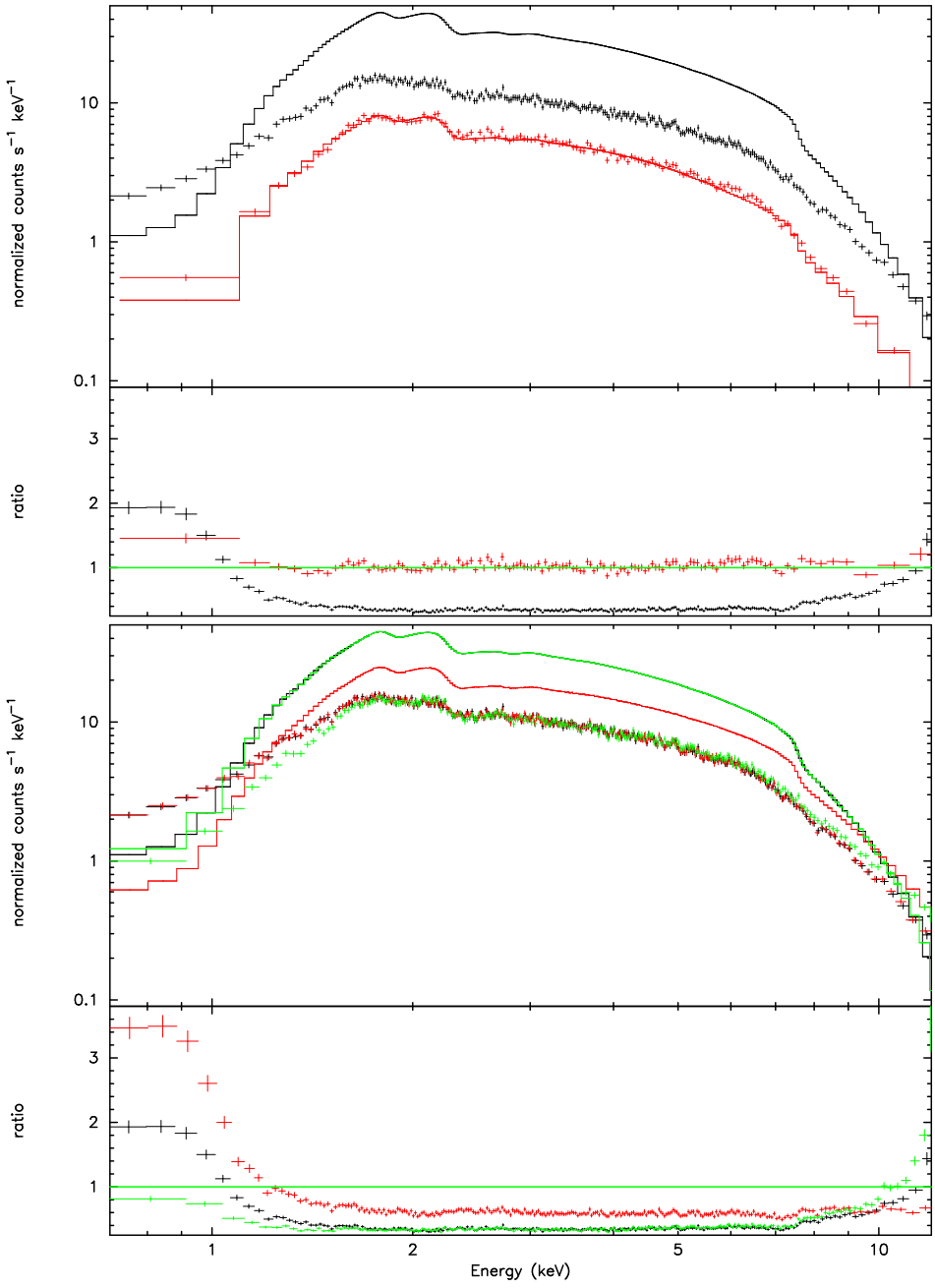

Figure 8: SAX J1711.6-3808 spectra and data-to-model residuals. The model used is that obtained from the best fit to the annular region data (the data have been binned to a signal-to-noise ratio of 20 for clarity). *Top panel:* SAX J1711.6-3808 spectra obtained from a circular (black) and annular (red) extraction region. The circular region spectrum is clearly distorted due to the combined effects of PU and XRL in the PSF core. *Bottom panel:* SAX J1711.6-3808 spectra obtained from a circular extraction region: uncorrected (black), with PU correction only (red) and with XRL correction only (green).

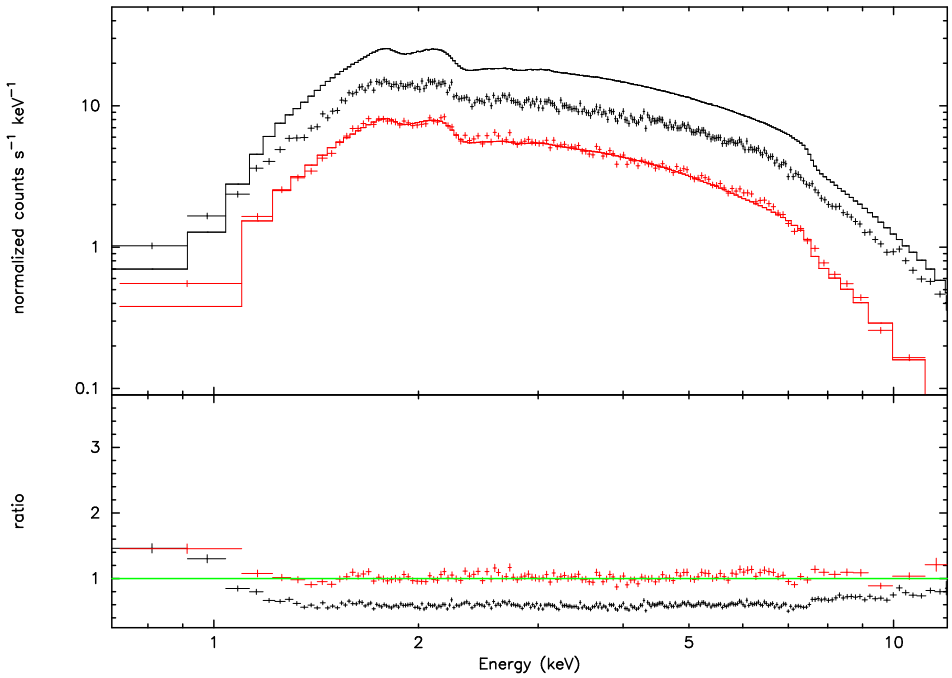

Figure 9: SAX J1711.6-3808 spectra obtained from an annular region (red) and from a circular region (black), the latter having been corrected for both XRL and PU. As before, the model used is that obtained from the best fit to the annular region data.

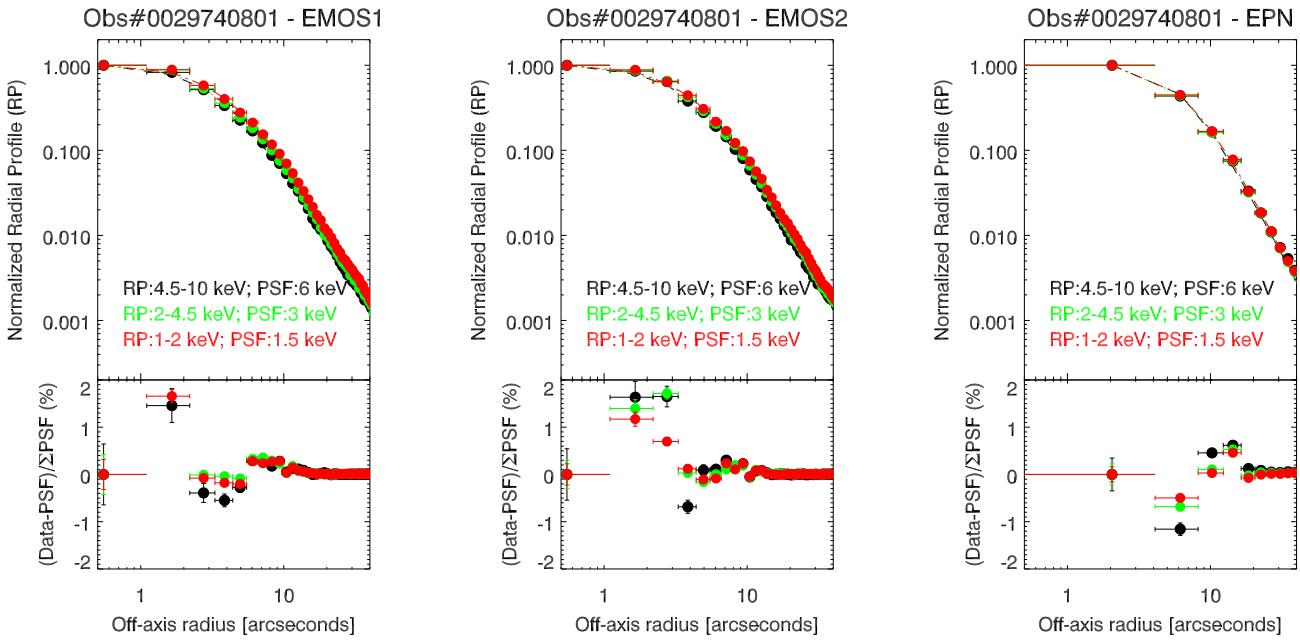

Figure 10: Comparison between the measured and the Point Spread Function (PSF) `ELLBETA` radial profile. *Upper panel*: profiles; *Lower panels*: difference between the observed and the PSF profile normalised to the integral of the former profile (in units of percent). *Colours* indicate different energy ranges as in the *inset labels*. The data are from Obs.#0029740801.

4.1.6 Test of new SAS tasks `multixmmselect`, `multiespecget`

Analysis of the source 1207+39W4 with `multixmmselect` and `multiespecget` have been performed, using simultaneously data from all 3 EPIC cameras, in two modalities: I) using only one ODF (ObsID 0112830201) and II) using 2 ODFs (ObsIDs 0112830201 and 0112830501) Both tests include:

- production of spectral products
- creating grouped spectral files to be used with XSPEC
- combined fit with XSPEC using individual spectral files and combined spectral files
- derivation of spectral fit parameters (using a power law model with absorption)
- production of ligth curves for each instrument

Results:
I - Analysis of 1 ODF
A comparison has taken place within XSPEC of spectral fits between:

A a combined fit to the individual instrument spectral files (1 pn, 1 MOS1 and 1 MOS2). For this comparison, specgroup has been run with no binning. . Cstatistics is used for fitting.

B a fit to the combined instrument spectral files with the combined response matrix. No binning has been applied since specgroup cannot run on combined spectral files. Cstatistics is used for fitting.

```
   A- Fit results:

========================================================================
Model TBabs<1>*powerlaw<2> Source No.: 1   Active/On
Model Model Component  Parameter  Unit     Value
 par  comp
   1    1   TBabs      nH         10^22    4.27677E-02  +/-  1.17871E-03
   2    2   powerlaw   PhoIndex            2.22635      +/-  9.33227E-03
   3    2   powerlaw   norm                1.85311E-03  +/-  1.21165E-05
------------------------------------------------------------------------


 Fit statistic  : C-Statistic =        5286.43 using 5875 PHA bins and 5872 DoF
 Test statistic : Chi-Squared =        6294.75 using 5875 PHA bins.
 Reduced chi-squared =        1.07199 for   5872 degrees of freedom
 Null hypothesis probability =   6.748083e-05

 Model Flux 0.00055222 photons (3.4066e-12 ergs/cm^2/s) range (2.0000 - 10.000 keV)
     Error range 0.0005441 - 0.0005600    (3.350e-12 - 3.464e-12)  (90.00% confidence)


 B- Fit results:
```

```
========================================================================
Model TBabs<1>*powerlaw<2> Source No.: 1   Active/On
Model Model Component  Parameter  Unit     Value
 par  comp
   1    1   TBabs      nH         10^22    4.16773E-02  +/-  1.17673E-03
   2    2   powerlaw   PhoIndex            2.21320      +/-  9.17272E-03
   3    2   powerlaw   norm                1.84549E-03  +/-  1.21106E-05
------------------------------------------------------------------------


 Fit statistic  : C-Statistic =        1990.63 using 1959 PHA bins and 1956 DoF
 Test statistic : Chi-Squared =        2414.90 using 1959 PHA bins.
 Reduced chi-squared =        1.23461 for   1956 degrees of freedom
 Null hypothesis probability =   3.925018e-12

 Model Flux 0.00055918 photons (3.4584e-12 ergs/cm^2/s) range (2.0000 - 10.000 keV)
     Error range 0.0005506 - 0.0005661    (3.397e-12 - 3.508e-12)  (90.00% confidence)
```

II. Analysis of 2 ODFs
Again, we compare spectral fits within XSPEC between:

A a combined fit to the individual instrument spectral files (2 pn, 2 MOS1 and 2 MOS2). For this comparison, specgroup has been run with no binning. Cstatistics is used for fitting.

B a fit to the combined instrument spectral files with the combined response matrix. No binning has been applied since specgroup cannot run on combined spectral files. Cstatistics is used for the fitting.

```
   A- Fit results:

========================================================================
Model TBabs<1>*powerlaw<2> Source No.: 1   Active/On
Model Model Component  Parameter  Unit     Value
 par  comp
   1    1   TBabs      nH         10^22    4.22289E-02  +/-  5.97124E-04
   2    2   powerlaw   PhoIndex            2.21183      +/-  4.66938E-03
   3    2   powerlaw   norm                1.84531E-03  +/-  6.16466E-06
------------------------------------------------------------------------


 Fit statistic  : C-Statistic =       11348.15 using 11750 PHA bins and 11747 DoF
 Test statistic : Chi-Squared =       16446.18 using 11750 PHA bins.
 Reduced chi-squared =       1.400032 for  11747 degrees of freedom
 Null hypothesis probability =  1.101464e-164
```

```
 Model Flux 0.00056004 photons (3.4647e-12 ergs/cm^2/s) range (2.0000 - 10.000 keV)
     Error range 0.0005565 - 0.0005634    (3.438e-12 - 3.492e-12)  (90.00% confidence)


   B- Fit results:

========================================================================
Model TBabs<1>*powerlaw<2> Source No.: 1   Active/On
Model Model Component  Parameter  Unit     Value
 par  comp
   1    1   TBabs      nH         10^22    4.19853E-02  +/-  6.03131E-04
   2    2   powerlaw   PhoIndex            2.20778      +/-  4.66065E-03
   3    2   powerlaw   norm                1.84379E-03  +/-  6.21400E-06
------------------------------------------------------------------------


 Fit statistic  : C-Statistic =        2122.82 using 1959 PHA bins and 1956 DoF
 Test statistic : Chi-Squared =        2741.07 using 1959 PHA bins.
 Reduced chi-squared =        1.40137 for   1956 degrees of freedom
 Null hypothesis probability =   2.237271e-29

 Model Flux 0.00056244 photons (3.4824e-12 ergs/cm^2/s) range (2.0000 - 10.000 keV)
     Error range 0.0005591 - 0.0005660    (3.459e-12 - 3.509e-12)  (90.00% confidence)
```

Conclusions:
All the files produced by `multixmmselect` are correct in the sense that they can be further manipulated or visualised without problems. This includes both spectral files and light curve files. The only issue found is that the combined instrument spectral files can not be grouped using specgroup since these files are no longer instrument dependent.
Within XSPEC, a power law model with absorption has been fitted to the combined instrument spectral files, and to the combination of individual instrument spectral files. The test has been carried out on a single odf and on the combination of two odfs. The results have been compared in terms of agreement between the derived fitted model parameters.
The derived spectral slopes agree to within 1%.
The derived fluxes agree to within 2%.
Despite the very good agreement shown here, we keep from first principles that co-addition is a valid procedure for fast derivation of results but should be handled with care when computing systematic errors. Since all individual spectra are derived with their corresponding response matrices the most accurate simultaneous fitting is always possible and recommended.
Comments

- the individual images for each instrument produced automatically by OGIP Spectral Products are not filtered and are only indicative. The mosaic image on the contrary is a final filtered product, done the same way as the spectral products.
- the task `specgroup` cannot be run on the combined spectral files for further analysis in XSPEC

- testing the spectral files in XSPEC:
  - files load ok, both in the case of individual instrument files and those corresponding to the combined spectrum
  - a combined fit to all the individual instrument files produces consistent results

4.1.7 Validation of the heliocentric and Sun Angle corrections to the RGS wavelength scale

The dataset used in this work was the same as in previous studies of the RGS Wavelength scale (see XMM-SOC-CAL-0098 and 0101): 109 exposures (59 for RGS1, 60 for RGS2) of the four wavelength calibrators, AB Dor, Capella, HR 1099 and Procyon, obtained between March 2000 and August 2010.
All data were processed with xmmsas_20130305_1802 and the CCFs RGS1_SAACORR_0001.CCF and RGS2_SAACORR_0001.CCF.
The results have been compared to those obtained with SAS12.1 in April 2012 for the validation of implementation of the Variable Boresight for RGS. All the measurements are corrected for the velocity of the objects.
Two caveats:

- CAVEAT 1: the same SA correction has been used for 1st and 2nd order (different for RGS1 and RGS2). As a consequence the accuracy of the applied Sun Angle correction for 2nd order spectra is lower.
- CAVEAT 2: the only difference in the processing with respect to SAS12 is the use of response matrices with 4000 energy channels, instead of 1000 as was done previously. The reason is that in the SAS13 version used here the response matrices obtained with a non-default value of the number of energy channels shows wiggles that distort the fluxed spectra and can affect the measurement of the line positions.

Data were processed with SAS13 using four different options:

- Set a) withheliocentriccorr = no & withsunanglecorr = no
- Set b) withheliocentriccorr = yes & withsunanglecorr = no
- Set c) withheliocentriccorr = no & withsunanglecorr = yes
- Set d) withheliocentriccorr = yes & withsunanglecorr = yes

Table 4: SAS 12.0.1 vs. SAS 13 without any correction

Average shifts per spectrum (mÅ)

	SAS12	SAS13a	SAS12-SAS13a
RGS1 o1	2 ± 6	2 ± 6	0 ± 1
RGS2 o1	8 ± 6	8 ± 6	0 ± 1
RGS1 o2	2 ± 3	3 ± 3	0 ± 1
RGS2 o2	3 ± 4	3 ± 4	0 ± 1
Order 1 - Order 2			
RGS 1	1 ± 4	1 ± 4	
RGS 2	4 ± 4	4 ± 4	
RGS 1 - RGS 2			
Order 1	-5 ± 2	-5 ± 2	
Order 2	-2 ± 2	-2 ± 1	

Shifts of individual lines (mÅ)

	SAS12	SAS13a	SAS12-SAS13a
RGS1 o1	2 ± 7	2 ± 7	0 ± 1
RGS2 o1	7 ± 7	7 ± 7	0 ± 1
RGS1 o2	1 ± 5	2 ± 5	0 ± 2
RGS2 o2	3 ± 4	3 ± 4	0 ± 1

==>There is not any systematic difference between the wavelengths measured in the spectra obtained with SAS12.0.1 and SAS13 without applying any of the new corrections.

II. Comparison of the data sets processed with different options

* Heliocentric correction

Table 5: SAS 13 results without and with heliocentric correction

Average shifts per spectrum (mÅ)

	SAS13a	SAS13b
RGS1 o1	2 ± 6	3 ± 6
RGS2 o1	8 ± 6	8 ± 6
RGS1 o2	3 ± 3	2 ± 3
RGS2 o2	3 ± 4	3 ± 4

Shifts of individual lines (mÅ)

	SAS13a	SAS13b
RGS1 o1	2 ± 7	2 ± 7
RGS2 o1	7 ± 7	8 ± 7
RGS1 o2	2 ± 5	2 ± 5
RGS2 o2	3 ± 4	3 ± 4

==> The heliocentric correction introduces very small changes in the wavelength scale.

*** SA correction**

Table 6: SAS 13 results without and with SA correction

Average shifts per spectrum (mÅ)

	SAS13a	SAS13c
RGS1 o1	2 ± 6	1 ± 5
RGS2 o1	8 ± 6	1 ± 5
RGS1 o2	3 ± 3	1 ± 3
RGS2 o2	3 ± 4	1 ± 3

Shifts of individual lines (mÅ)

	SAS13a	SAS13c
RGS1 o1	2 ± 7	1 ± 6
RGS2 o1	7 ± 7	1 ± 6
RGS1 o2	2 ± 5	1 ± 5
RGS2 o2	3 ± 4	0 ± 6

==> The Sun Angle correction aligns both RGSs and orders and decreases the scatter in the measurements.

**** heliocentric + SA corrections**

Table 7: SAS 13 results without any and with both corrections)

	SAS13a	SAS13d	
RGS1 o1	2 ± 6	1 ± 5	Average shifts / spectrum (mÅ)
RGS2 o1	8 ± 6	0 ± 5	
RGS1 o2	3 ± 3	1 ± 3	
RGS2 o2	3 ± 4	0 ± 2	

	SAS13a	SAS13d	
RGS1 o1	2 ± 7	0 ± 6	
RGS2 o1	7 ± 7	0 ± 6	Shifts of individual lines (mÅ)
RGS1 o2	2 ± 5	1 ± 5	
RGS2 o2	3 ± 4	0 ± 4	

==> The application of the two new corrections aligns both RGSs and orders and decreases the scatter in the measurements.

Table 8: Comparison of all samples

Average shifts per spectrum (mÅ)

	SAS13a	SAS13b	SAS13c	SAS13d
RGS1 o1	2 ± 6	3 ± 6	1 ± 5	1 ± 5
RGS2 o1	8 ± 6	8 ± 6	1 ± 5	0 ± 5
RGS1 o2	2 ± 3	2 ± 3	1 ± 3	1 ± 3
RGS2 o2	3 ± 4	3 ± 4	1 ± 3	0 ± 2
Order 1 - Order 2				
RGS 1	1 ± 4	1 ± 4	0 ± 4	0 ± 4
RGS 2	4 ± 4	4 ± 3	-1 ± 3	0 ± 3
RGS 1 - RGS 2				
Order 1	-5 ± 2	-5 ± 2	1 ± 3	1 ± 2
Order 2	-2 ± 1	-2 ± 1	1 ± 2	1 ± 2

Shifts of individual lines (mÅ)

	SAS13a	SAS13b	SAS13c	SAS13d
RGS1 o1	2 ± 7	2 ± 7	1 ± 6	0 ± 6
RGS2 o1	7 ± 7	8 ± 7	1 ± 6	0 ± 6
RGS1 o2	2 ± 5	2 ± 5	1 ± 5	1 ± 5
RGS2 o2	3 ± 4	3 ± 4	0 ± 6	0 ± 4

==> These results show the expected improvement.

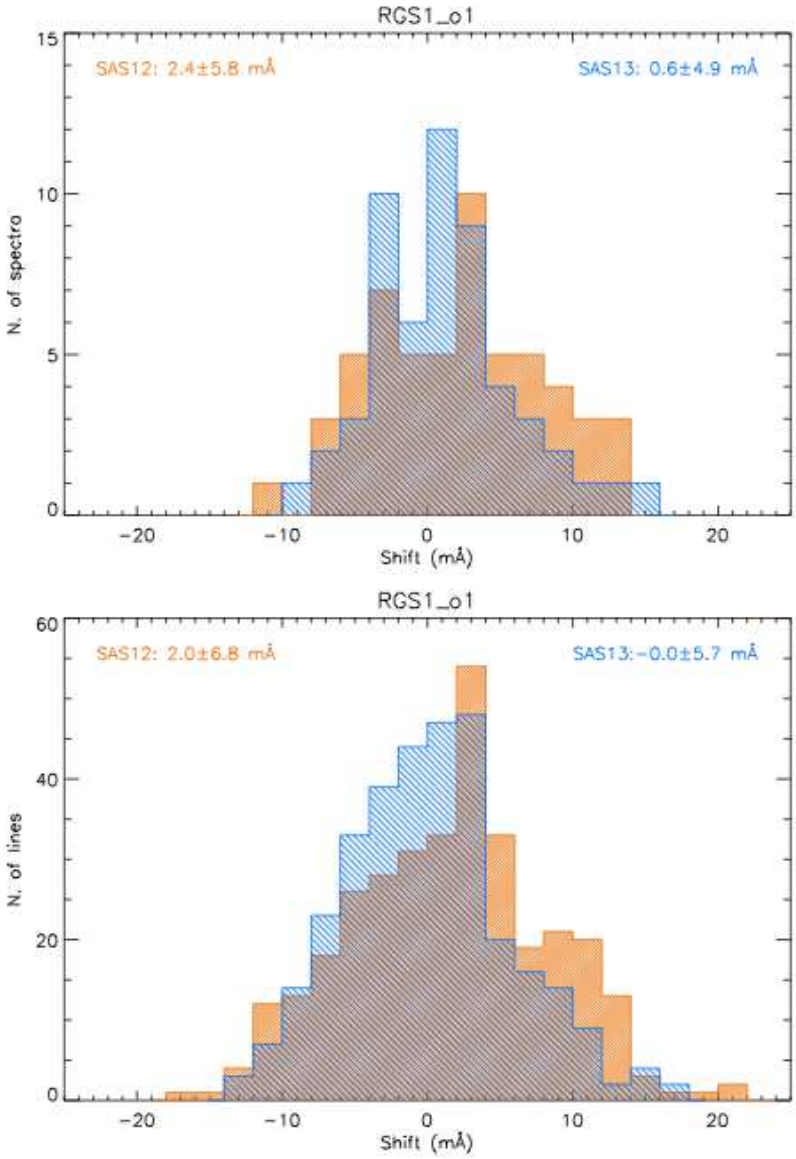

Figure 11: Wavelength shifts for spectra and single lines with SAS 12 and SAS 13 - RGS1 first order

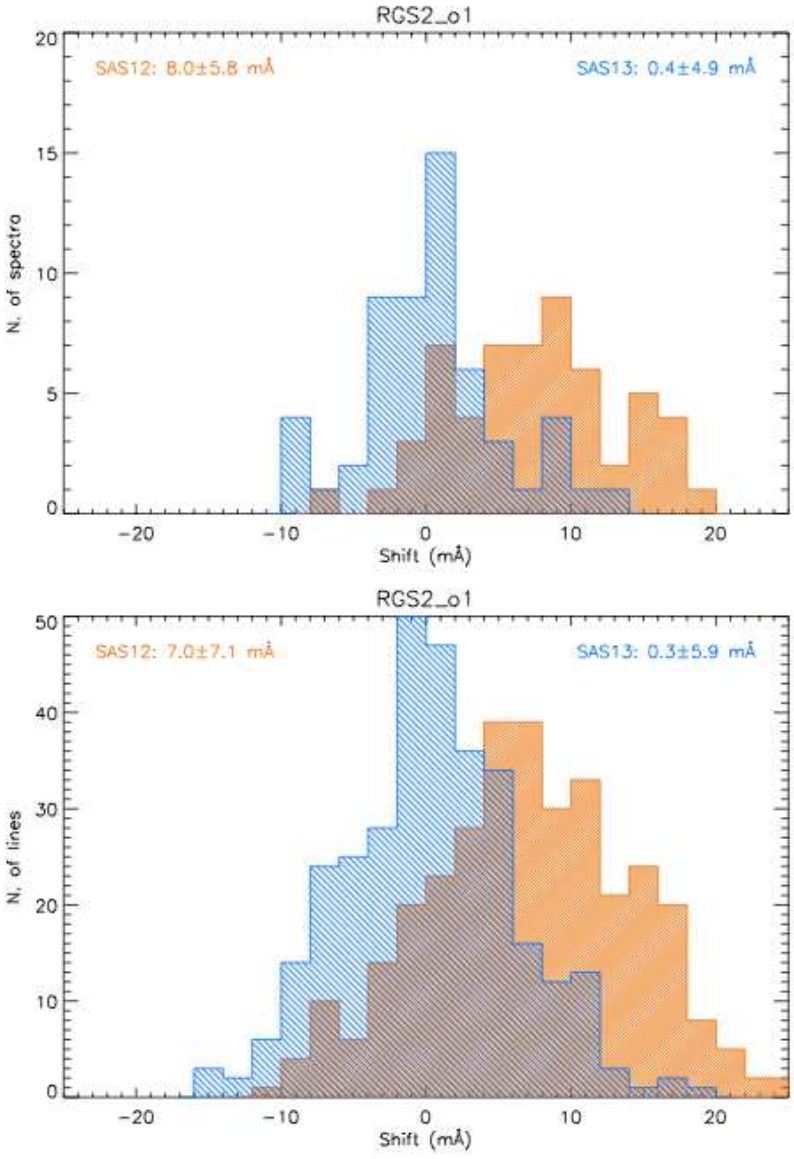

Figure 12: Wavelength shifts for spectra and single lines with SAS 12 and SAS 13 - RGS2 first order

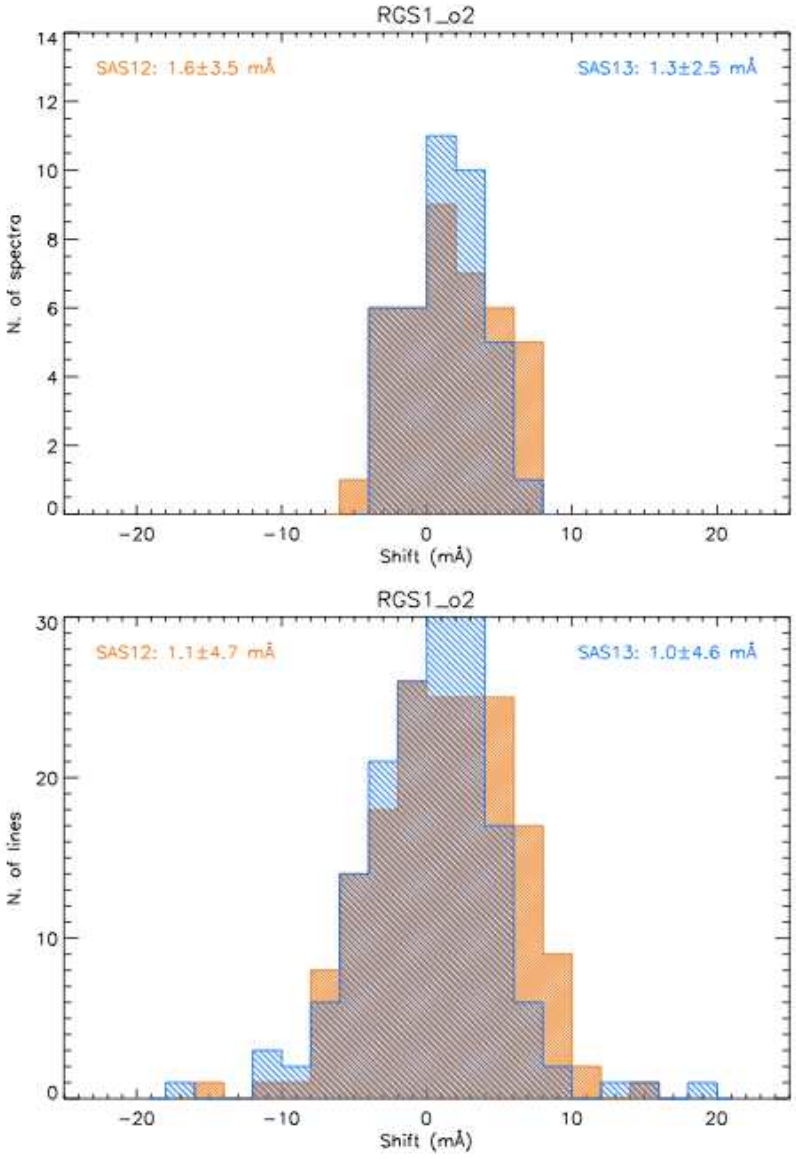

Figure 13: Wavelength shifts for spectra and single lines with SAS 12 and SAS 13 - RGS1 second order

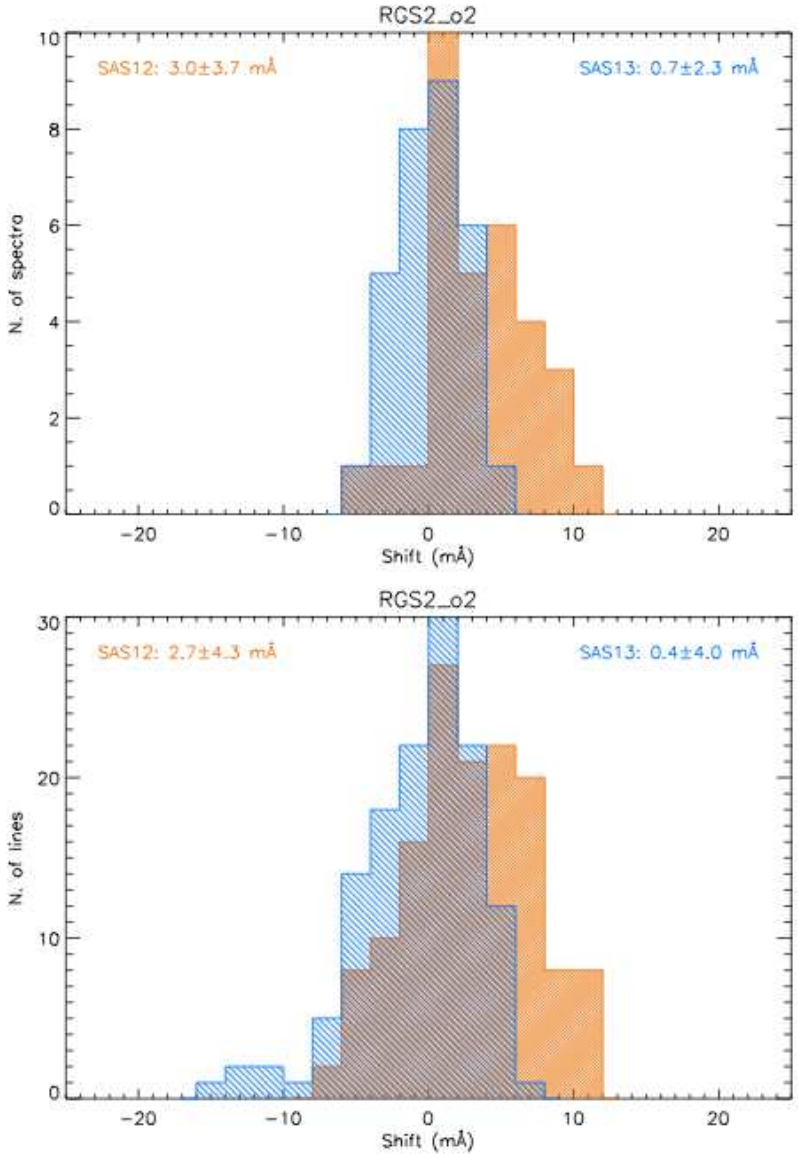

Figure 14: Wavelength shifts for spectra and single lines with SAS 12 and SAS 13 - RGS2 second order

IV. Further checks

a) Comparison of obsids 01347221 and 01347217: two observations of Capella taken at extreme SA values (108 and 73). Fig. 15 to 18 show the comparison of both RGS and orders processed with SAS12 and SAS13, the latter with corrections for heliocentric velocity and SA correlation.

Table 9: Shifts between spectra taken at extreme SA values - processed with SAS 12 and SAS 13 including corrections for heliocentric velocity and SA correlation (mÅ)

	SAS12	SAS13
RGS1 o1	22	2
RGS2 o1	23	5
RGS1 o2	12	3
RGS2 o2	15	6

==¿ The agreement between the wavelengths measured on both spectra improves from approx. 22 mÅto approx. 3 mÅfor 1st order (from 13 mÅto 4 mÅfor 2nd order). A small, intrinsic, shift due to orbital motion cannot be excluded.

b) Check with an observation of Capella (obsid 05107806 in rev 2163) that was not used in the derivation of the SA correlation, and was observed at a Solar Angle of 105.

4.1.8 SAS OM S/W validation

The specific OM validation was done in two ways:

- Analysis of the Validation Data Set processed with SAS 13

  Data sets were examined, both in 32 and 64 bits. A truncation in the file name of some output postscript files was produced in all data sets in the processing with `omichain`. Curiously, this problem was not seen when processing the same data in a normal workstation. It seems this is related to file and path names handling by pgplot. Apart from this, no problem was encountered in the revised data sets.

- Running SAS 13 in several data sets.

  Several standard stars were processed with SAS 13. The obtained results are satisfactory. It can be also mentioned that more than 6000 ODFs have been processed for the new release of the OM source catalog using a SAS 13 version.

Table 10: Average shift (mÅ) for Capella (obsid 05107806 in rev 2163), observed at a Solar Angle of 105 degrees

	SAS13a	SAS13b
RGS1 o1	-6 $\pm$ 3	2 $\pm$ 3
RGS2 o1	0 $\pm$ 1	3 $\pm$ 2
RGS1 o2	-4 $\pm$ 5	0 $\pm$ 5
RGS2 o2	5 $\pm$ 1	1 $\pm$ 2

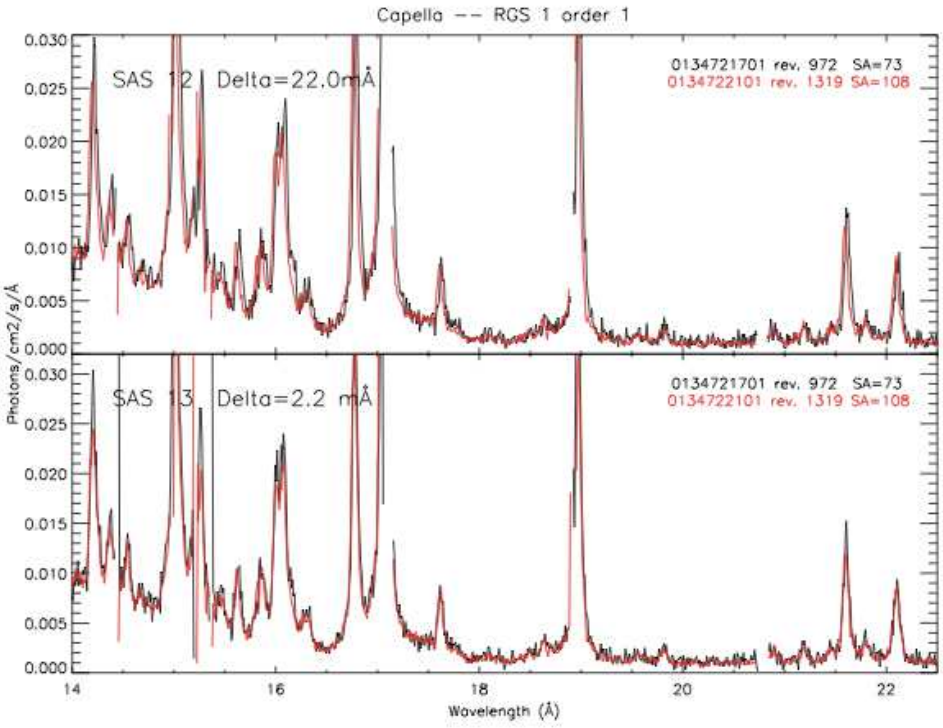

Figure 15: Comparison of data processed with SAS12 and SAS13, the latter including corrections for heliocentric velocity and SA correlation - RGS1 first order

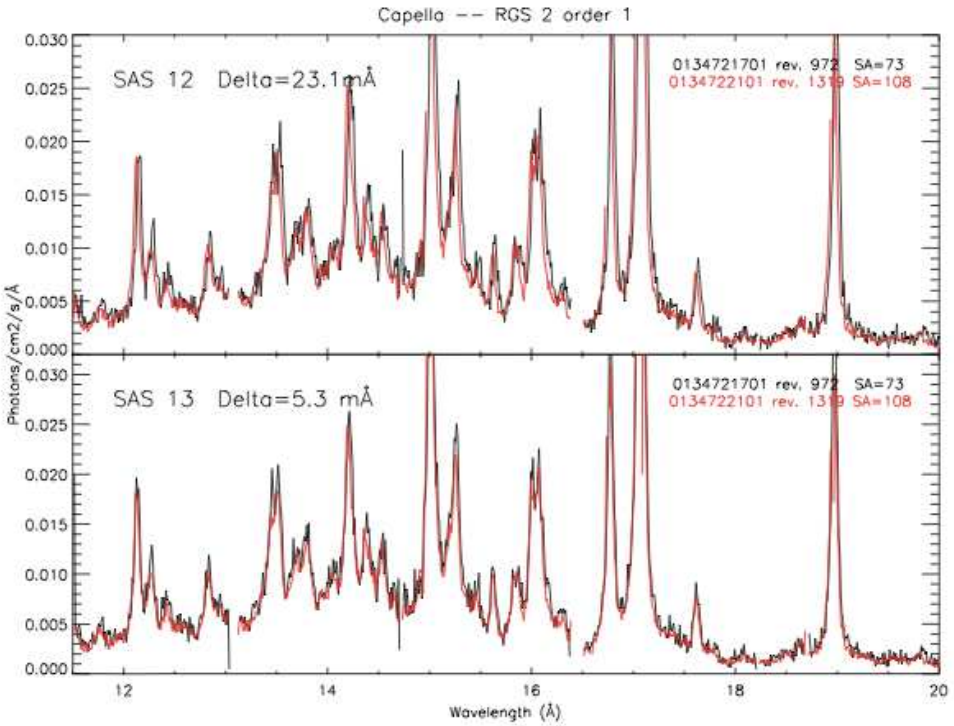

Figure 16: Comparison of data processed with SAS12 and SAS13, the latter including corrections for heliocentric velocity and SA correlation - RGS2 first order

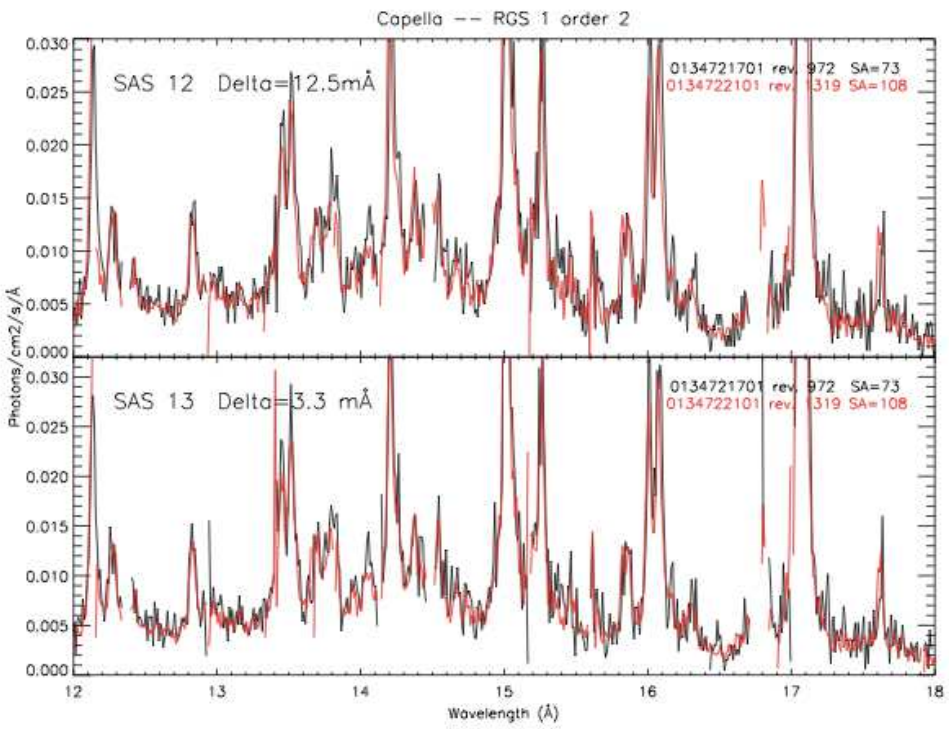

Figure 17: Comparison of data processed with SAS12 and SAS13, the latter including corrections for heliocentric velocity and SA correlation - RGS1 second order

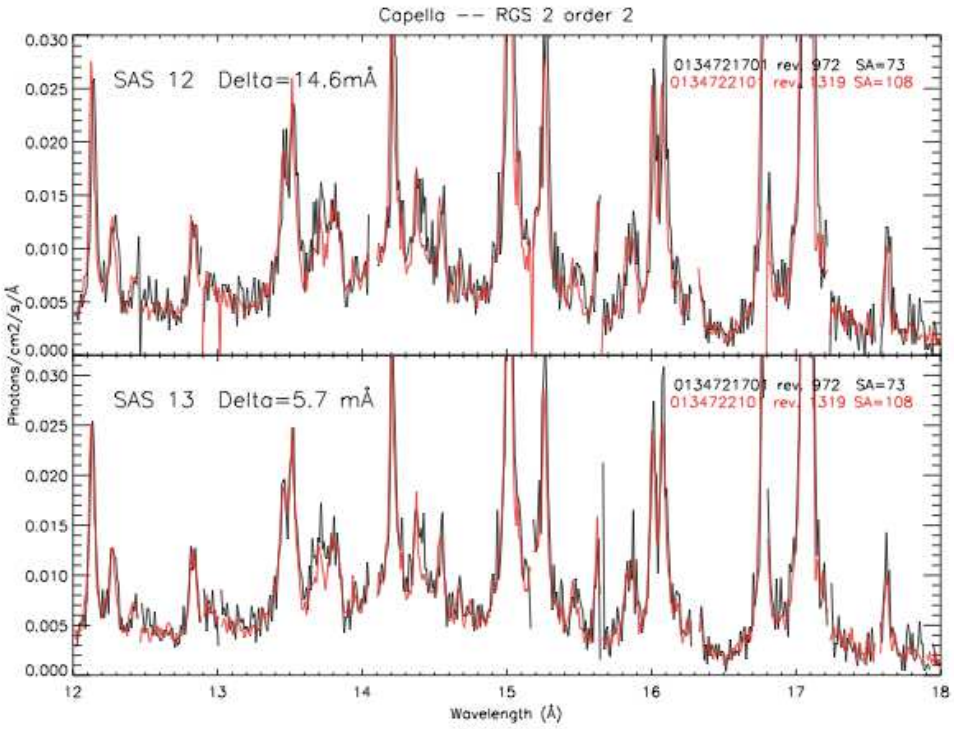

Figure 18: Comparison of data processed with SAS12 and SAS13, the latter including corrections for heliocentric velocity and SA correlation - RGS2 second order

4.2 SAS 13.5 validation

The standard validation has proceeded as planned, with the reduction of all the standard datasets via scripts based on `epicproc / rgsproc / om[i,g,f]chain`. Parallel versions of the pipeline including the original and an upgraded version of the `oal` package have been produced. The upgrade should only affect EPIC mosaic data, but the central role of such a task called for caution here and for reduction of a large number of datasets with both versions, followed by their comparison. They have been found to be identical. Also the XCal archive has been fully processed with SAS 13.5, the cross-calibration results have been taken for an upgrade of the Calibration Document. Special attention was paid to the interactive analysis and the new / updated features dedicated analysis, this time including also running all individual analysis threads, to insure the full functionality contained in them and at the same time their validity. SAS 13.5 was finally released, with less than 2 weeks delay wrt the original plan on December 11 2013.
There were no errors in any of the reductions, neither with the "procs" nor with the SAS 13.5 based pipelines. The results from the cross-calibration exercise are considered globally fully acceptable and can be consulted through the Cross Calibration Review tool (http://xmm2.esac.esa.int/cgi-bin/ept/preview.pl). Reports on the interactive analysis performed for validation follow below.

4.2.1 Analysis results of PKS0558-504 data with SAS 13.0 and SAS 13.5

PKS0558-504, 0125110101 Rev 84

Table 11: PKS0558-504 (Rev 84) best fit parameters for a power law plus two black body model. The temperature of BB_1 is fixed to 150 eV. Data processed by SAS 13.0

Instrument	Γ	Norm_{BB1}	kT_{BB2}	Norm_{BB2}	$\mathrm{Flux}_{0.2-2keV}$	$\mathrm{Flux}_{2-10keV}$	χ^2/dof
-	-	10^{-5}	keV	10^{-5}	10^{-11} erg cm^{-2} s^{-1}		-
pn	$2.18^{+0.06}_{-0.06}$	$9.4^{+1.5}_{-1.7}$	$0.066^{+0.004}_{-0.003}$	32^{+4}_{-3}	$2.28^{+0.02}_{-0.01}$	$0.9^{+0.02}_{-0.02}$	75/100
MOS1	$2.18^{+0.09}_{-0.08}$	$8.9^{+2.1}_{-2.4}$	$0.066^{+0.006}_{-0.005}$	34^{+6}_{-5}	$2.29^{+0.02}_{-0.03}$	$0.9^{+0.02}_{-0.05}$	93/96
MOS2	$2.20^{+0.09}_{-0.08}$	$8.6^{+2.1}_{-2.3}$	$0.065^{+0.005}_{-0.005}$	35^{+6}_{-5}	$2.28^{+0.01}_{-0.03}$	$0.9^{+0.04}_{-0.04}$	113/103

Table 12: PKS0558-504 (Rev 84) best fit parameters for a power law plus two black body model. The temperature of BB_1 is fixed to 150 eV. Data processed by SAS 13.5

Instrument	Γ	Norm_{BB1}	kT_{BB2}	Norm_{BB2}	$\mathrm{Flux}_{0.2-2keV}$	$\mathrm{Flux}_{2-10keV}$	χ^2/dof
-	-	10^{-5}	keV	10^{-5}	10^{-11} erg cm^{-2} s^{-1}		-
pn	$2.18^{+0.07}_{-0.06}$	$9.4^{+1.54}_{-1.65}$	$0.065^{+0.003}_{-0.003}$	$33^{+4}_{-3.6}$	$2.28^{+0.01}_{-0.02}$	$0.9^{+0.02}_{-0.02}$	84/101
MOS1	$2.15^{+0.08}_{-0.08}$	$9.5^{+2.10}_{-2.36}$	$0.066^{+0.005}_{-0.005}$	$35^{+6}_{-5.2}$	$2.29^{+0.03}_{-0.03}$	$0.9^{+0.03}_{-0.03}$	102/100
MOS2	$2.21^{+0.09}_{-0.08}$	$8.4^{+2.09}_{-2.32}$	$0.064^{+0.005}_{-0.004}$	$37^{+6}_{-5.5}$	$2.30^{+0.02}_{-0.03}$	$0.8^{+0.03}_{-0.03}$	102/100

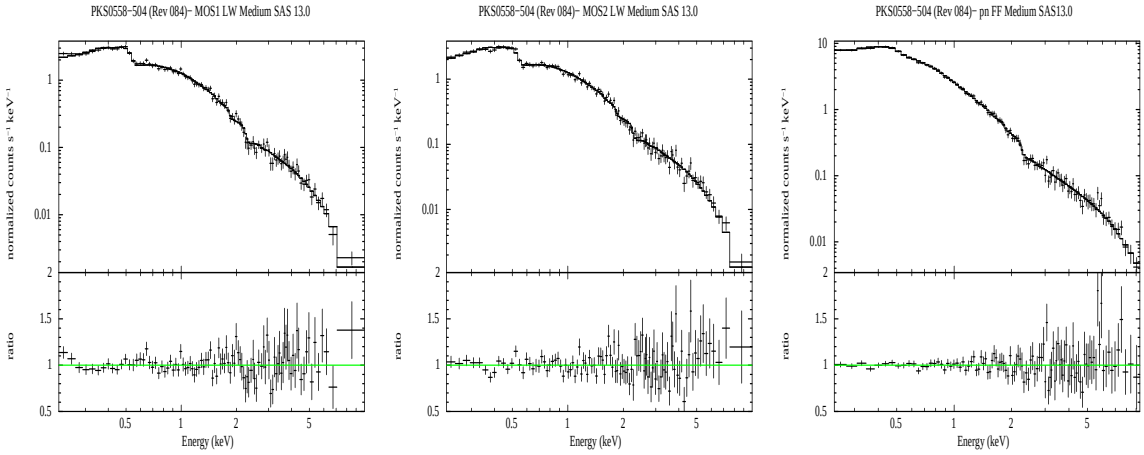

Figure 19: Spectra and residuals of PKS0558-504 (Rev 84) after excision of the PSF core. Data have been processed by SAS 13.0

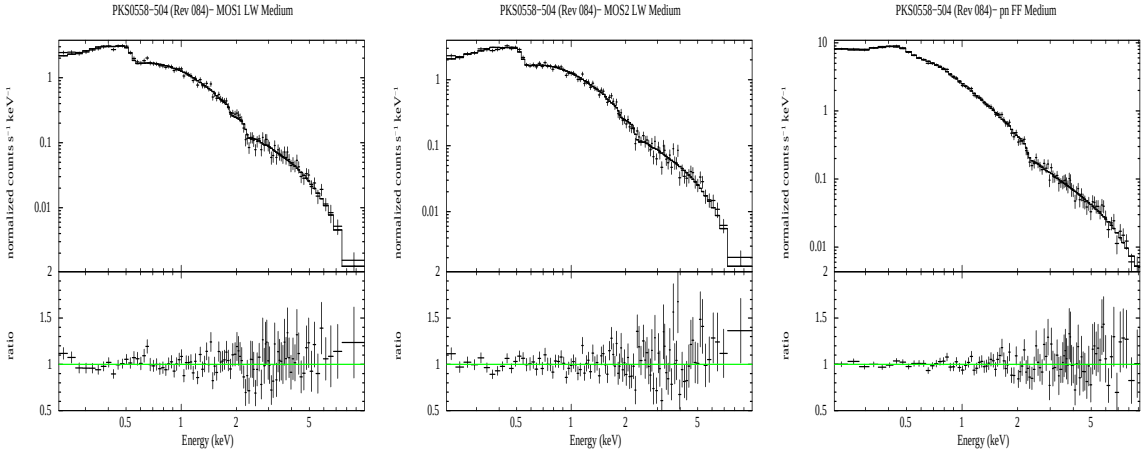

Figure 20: Spectra and residuals of PKS0558-504 (Rev 84) after excision of the PSF core. Data have been processed by SAS 13.5

PKS0558-504, 0129360201 Rev 153

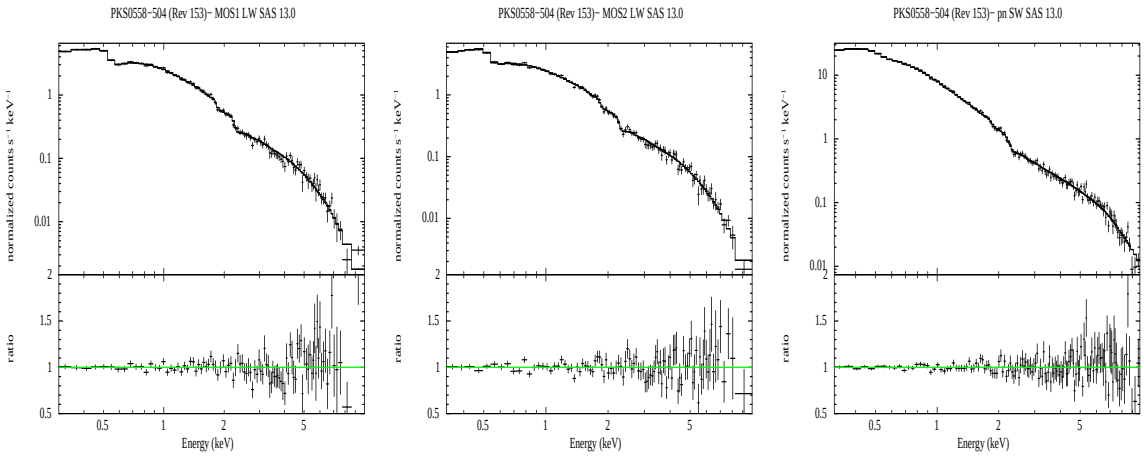

Figure 21: Spectra and residuals of PKS0558-504 (Rev 153). Data have been processed by SAS 13.0

Table 13: PKS0558-504 (Rev 153) best fit parameters for a power law plus two black body model. Data processed by SAS 13.0

Inst	Γ	kT_{BB1}	$Norm_{BB1}$	kT_{BB2}	$Norm_{BB2}$	$Flux_{0.2-2keV}$	$Flux_{2-10keV}$	χ^2/dof
-	-	keV	10^{-5}	keV	10^{-5}	10^{-11} erg cm^{-2} s^{-1}		-
pn	$2.16^{+0.04}_{-0.04}$	$0.15^{+0.008}_{-0.007}$	$12^{+1.1}_{-1.1}$	$0.058^{+0.003}_{-0.003}$	36^{+3}_{-2}	$2.61^{+0.01}_{-0.01}$	$1.17^{+0.01}_{-0.01}$	136/130
MOS1	$2.15^{+0.06}_{-0.06}$	$0.14^{+0.012}_{-0.012}$	$11^{+1.6}_{-1.6}$	$0.061^{+0.004}_{-0.005}$	30^{+3}_{-3}	$2.52^{+0.01}_{-0.01}$	$1.20^{+0.03}_{-0.02}$	106/94
MOS2	$2.26^{+0.05}_{-0.04}$	$0.11^{+0.012}_{-0.009}$	$14^{+2.4}_{-3.1}$	$0.043^{+0.011}_{-0.011}$	$38^{+0.001}_{-0.001}$	$2.60^{+0.01}_{-0.05}$	$1.20^{+0.02}_{-0.02}$	111/95

Table 14: PKS0558-504 (Rev 153) best fit parameters for a power law plus two black body model. Data processed by SAS 13.5

Inst	Γ	kT_{BB1}	$Norm_{BB1}$	kT_{BB2}	$Norm_{BB2}$	$Flux_{0.2-2keV}$	$Flux_{2-10keV}$	χ^2/dof
-	-	keV	10^{-5}	keV	10^{-5}	10^{-11} erg cm^{-2} s^{-1}		-
pn	$2.16^{+0.04}_{-0.04}$	$0.14^{+0.008}_{-0.007}$	$12^{+1.02}_{-1.03}$	$0.058^{+0.003}_{-0.003}$	$36^{+2.9}_{-2.7}$	$2.6^{+0.006}_{-0.009}$	$1.1^{+0.01}_{-0.01}$	128/134
MOS1	$2.16^{+0.06}_{-0.06}$	$0.15^{+0.012}_{-0.012}$	$11^{+1.6}_{-1.6}$	$0.061^{+0.004}_{-0.004}$	$30^{+3.4}_{-3.5}$	$2.5^{+0.01}_{-0.01}$	$1.2^{+0.03}_{-0.02}$	106/94
MOS2	$2.26^{+0.04}_{-0.04}$	$0.11^{+0.012}_{-0.009}$	$14^{+2.4}_{-3.1}$	$0.043^{+0.011}_{-0.011}$	$38^{+0.001}_{-0.001}$	$2.6^{+0.006}_{-0.05}$	$1.2^{+0.02}_{-0.02}$	111/95

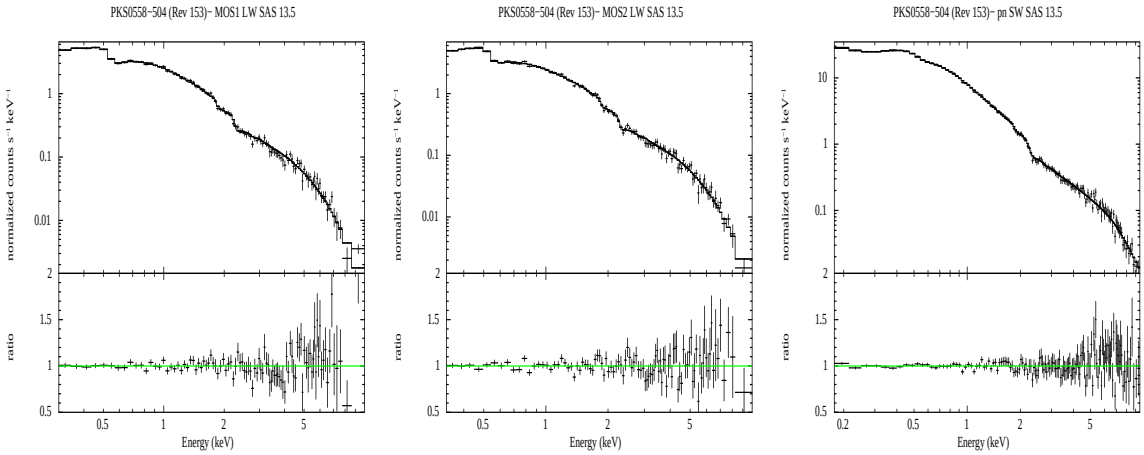

Figure 22: Spectra and residuals of PKS0558-504 (Rev 153). Data have been processed by SAS 13.5

4.2.2 G21.5 analysis - SAS 13.5

The early observation (April 2000) of the non-thermal SNR G21.5-0.9 (Obs.#0122700101) was included in the SAS Science Validation (SAS-SV) datasets since the beginning of the science validation exercise (Gabriel et al. 2001, available at:
`http://xmm.esac.esa.int/external/xmm_data_analysis/sas_validation/sas_sv51.shtml`).
More recently, a cross-calibration study involving all major X-ray operational missions was published in the framework of the IACHEC (International Consortium for High-Energy Calibration: `http://web.mit.edu/iachec/`) (Tsujimoto et al. 2011). G21.5-0.9 is a suitable source for effective area and cross-calibration studies due to its simple power-law, hard X-ray spectrum over a wide energy range, its flux stability, and its relative compactness (<1 arc-minute). Readers are refereed to the Tsujimoto et al. 2011 paper and references therein for a summary of the main X-ray properties of this source.
Data reduction and spectral analysis of the data described in this report followed the procedure as described in, *e.g.* Gabriel at al. 2008(available at:
`http://xmm.esac.esa.int/external/xmm_data_analysis/sas_validation/reports/SAS60_report.ps.gz`). Spectra and associated responses were extracted from a common region in the sky defined by `AND`-merging the instrument masks of the three EPIC cameras. The results of the spectral analysis, expressed through the parameters of a simple power-law model absorbed by a screen of photoelectric absorption over the whole EPIC sensitive energy bandpass, are summarised in Fig. 23. They are in agreement with

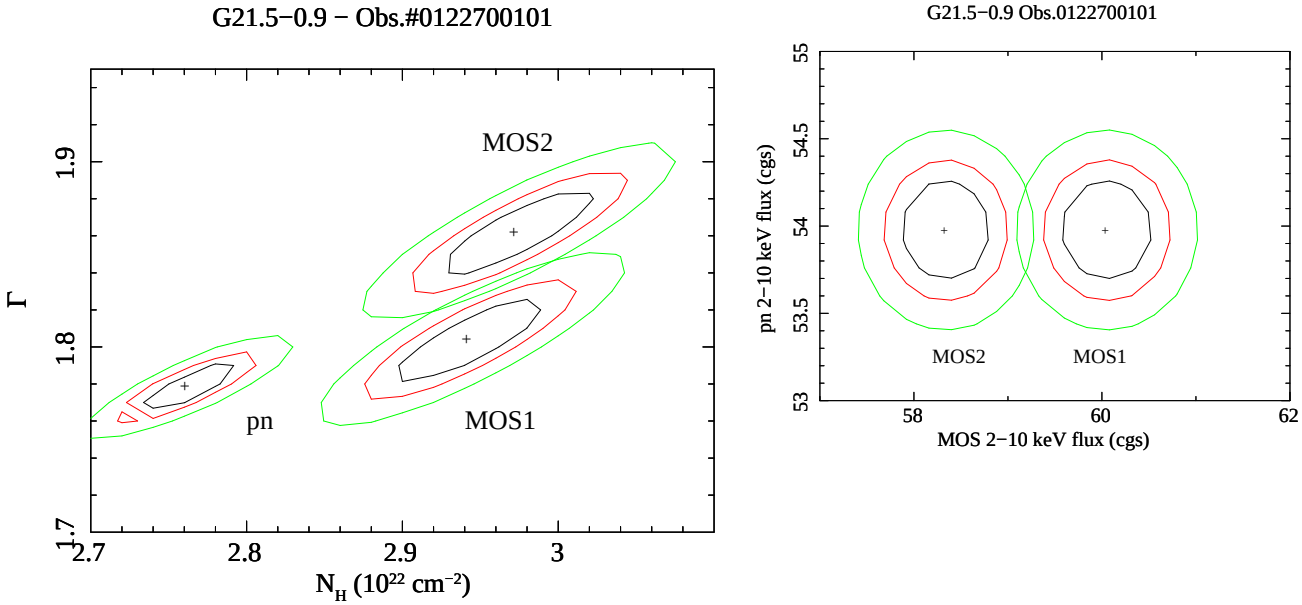

Figure 23: *Left panel*: iso-χ^2 contours for the column density versus the photon index when a simple photoelectrically absorbed power-law model is applied to the EPIC spectra of G21.5-0.9 in Obs.#0122700101. The contours indicate the 68%, 90% and 99% confidence levels for two interesting parameters. *Right panel*: the same for the 2–10 keV absorption corrected fluxes.

previous SAS-SV studies. This is expected, because the main EPIC-related calibration changes in SASv13.5 (the implementation of the MOS contamination and the corresponding update of the quantum efficiency and redistribution calibration files) affect only marginally the spectral results above 2 keV. However, the new effective area and redistribution calibration provides a better (albeit still not perfect) description of the EPIC-MOS spectrum red-wards the photo-electric cut-off, where the counts are dominated by the photon redistribution (Fig. 24). of this report for an analysis of the systematic uncertainties associated with the MOS effective area and redistribution calibrations after SASv13.5.

4.2.3 EPIC-MOS contamination model

The new EPIC-MOS contamination model and the corresponding corrections to the detector responses were verified within the SASv13.5 test run of the XMM-Newton SOC cross-calibration archive (XCAL) using 223 observations of 27 targets of various source types. Two specific results will be presented in the following section.

Due to its very soft X-ray emission and spectral stability, the monitoring of the isolated neutron star RXJ1856.6-3754 is a sensitive test case for low energy calibration. With SASv13.5 two different detector characteristics are taken into account: the time and spatial dependent degradation of spectral resolution in the detector response due to radiation damages around the bore-sight positions (EMOS patch) and the time dependent increasing absorption due to a growing layer of contaminant on the CCD. In SASv13.0 the patch correction partially compensated the effects of the so far unknown contamination.

Fig. 25 presents for 27 exposures of RXJ1856.6-3754 the comparison of the three parameters of an absorbed single blackbody model, N_H, temperature and normalisation. Using SASv13.5, the standard deviations for all three parameters decrease, proving that the monitoring results are

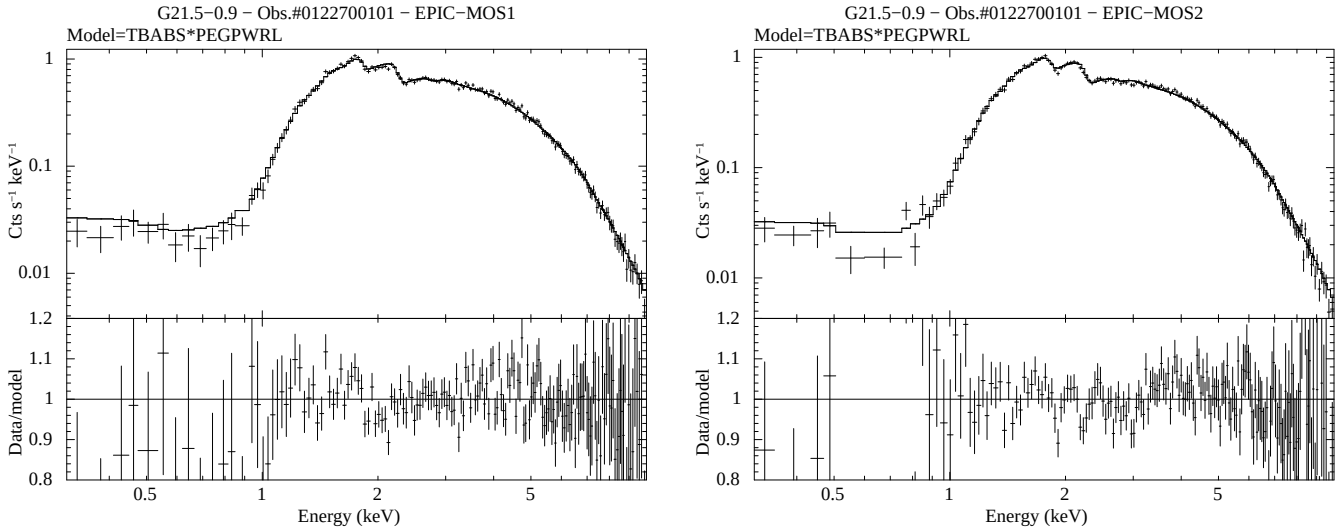

Figure 24: *Left panel*: Spectra (*top panel* and residuals in units of data/model ratio (*bottom panel*) when a photoelectrically absorbed power-law model is applied to the EPIC-MOS1 spectrum of G21.5-0.9. Each data point was binned to a signal-to-noise ratio >3 for plotting purposes only. *Right panel*: the same for EPIC-MOS2.

more stable than with SASv13.0.

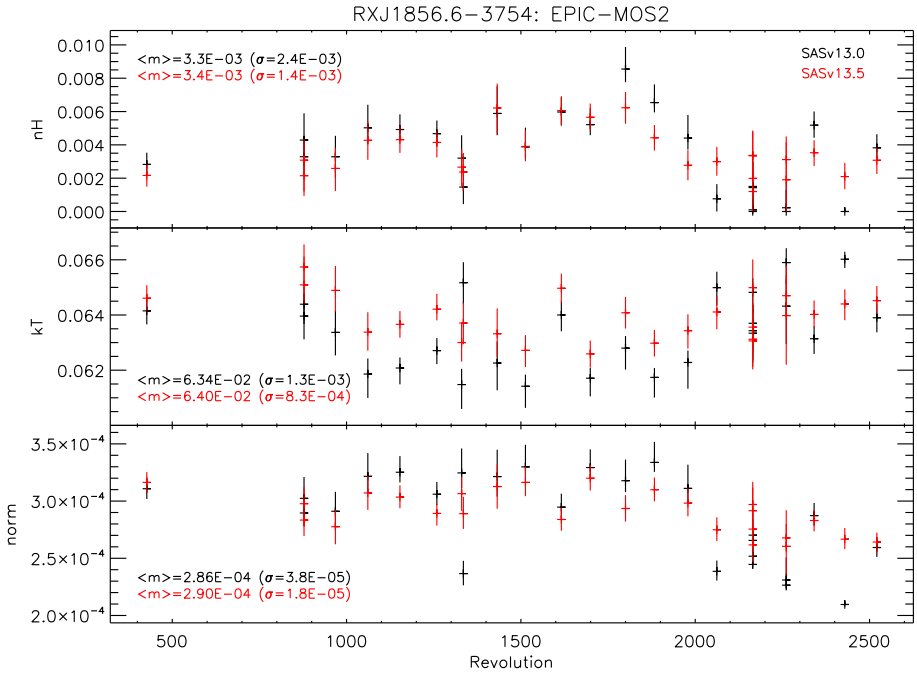

Figure 25: Comparison of N_H, temperature and normalisation of absorbed single blackbody model between SASv13.0 and SASv13.5

Fig. 26 compares the results of all XMM-Newton instruments (black:EPN, red: EMOS1, green: EMOS2, navy blue: RGS1, cyan: RGS2) for the 0.33-0.54 keV energy band flux ratios of XCAL

continuum sources using SASv13.0 and SASv13.5. Using the latter, the means of the EMOS flux ratio distributions increased and are closer to EPN than for the previous SAS version, proving a low energy flux increase of the EMOS due to the contamination correction.

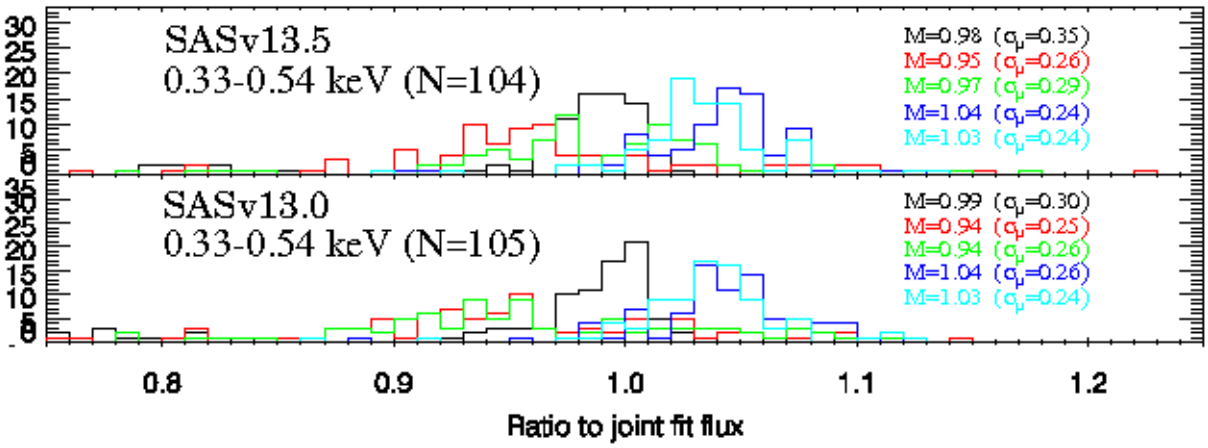

Figure 26: Results from all XMM-Newton X-ray instruments in soft band

4.2.4 Tests of RGS `rgsbkgmodel` fix

Fix in `rgsbkgmodel` to compute correctly the weighting factors in the observations with gaps in the CCD9 background light curve.

- Version tested: `rgsbkgmodel-1.4 [xmmsas_20131030_1901-13.5.0]`
- Procedure:

  RGS Background templates have been generated with SAS 13.5 for 40 ODFs having gaps in the CCD9 background light curve. They have been compared to the templates derived using SAS 13.0.

- Results

  In SAS 13.0 the weighting factor for the lowest template level was overestimated in the observations in which the light curve of CCD9 had gaps. This factor is now computed correctly, as the zero values in the CCD9 light curve are not taken into account any more.

  As a consequence of this change, in these cases the new background templates are higher than the previous ones, with the difference depending on the specific case.

  To check that the changes in the code did not affect other cases, new background models for a number of random observations have been compared with the results of previous SAS versions, without finding significant differences.

4.2.5 Test of RGS `rgsangles` task fix

Fix in `rgsfilter` to align exposure maps when applying corrections to the wavelength scale.

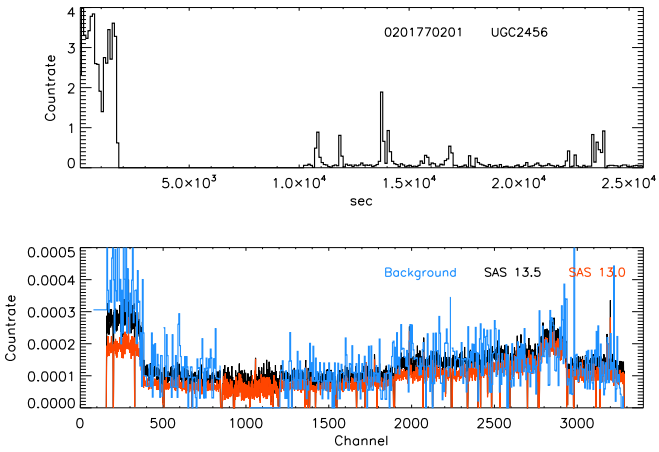

Figure 27: Example of background templates for an RGS1 observation with gaps in the CCD9 background lightcurve (top panel: background light curve, bottom: templates computed with SAS 13.0 (red) and SAS 13.5 (black) and, for comparison, background extracted from the observation (blue).)

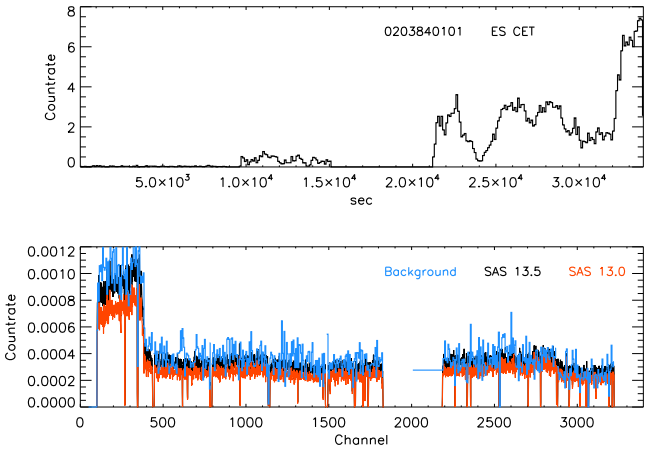

Figure 28: Same as the previous figure, but for an RGS2 observation.

- Reported in October 2013
- Version tested: `rgsfilter-1.18.2 [xmmsas_20131105_1901-13.5.0]`
- Procedure:

  Three ODFs have been processed with SAS 13.5: the one for which the problem was reported (0510781201, Capella) and two observations of Mkn 421 (0658800801 and 0162960101).

  The data were processed with four options: without any correction to the wavelength scale, with heliocentric velocity correction, with Sun angle correction, and with both corrections. Results were compared to similar processing with SAS 13.0.

- Results:

  The results of the processing with SAS 13.5 are fully satisfactory. The outliers that were seen in the data processed with SAS 13.0 when wavelength corrections were applied, do not appear using the new version of `rgsfilter`.

  As a consistency check, there are no differences between the spectra produced with both versions of SAS when no correction is applied.

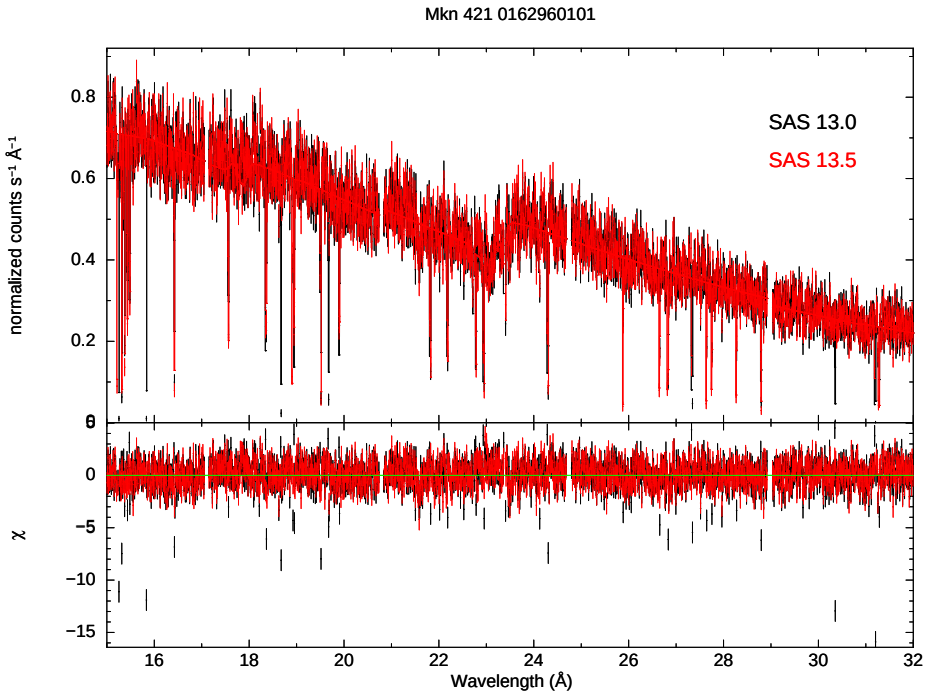

Figure 29: XSPEC fit to an absorbed powerlaw of one spectrum of Mkn 421, to which the heliocentric velocity correction was applied. The large number of outliers seen in the residuals of the fit of the spectrum processed with SAS 13.0 (i.e `rgsfilter-1.18.1`) disappear when using the new version of rgsfilter`rgsfilter-1.18.2` implemented in SAS 13.5.

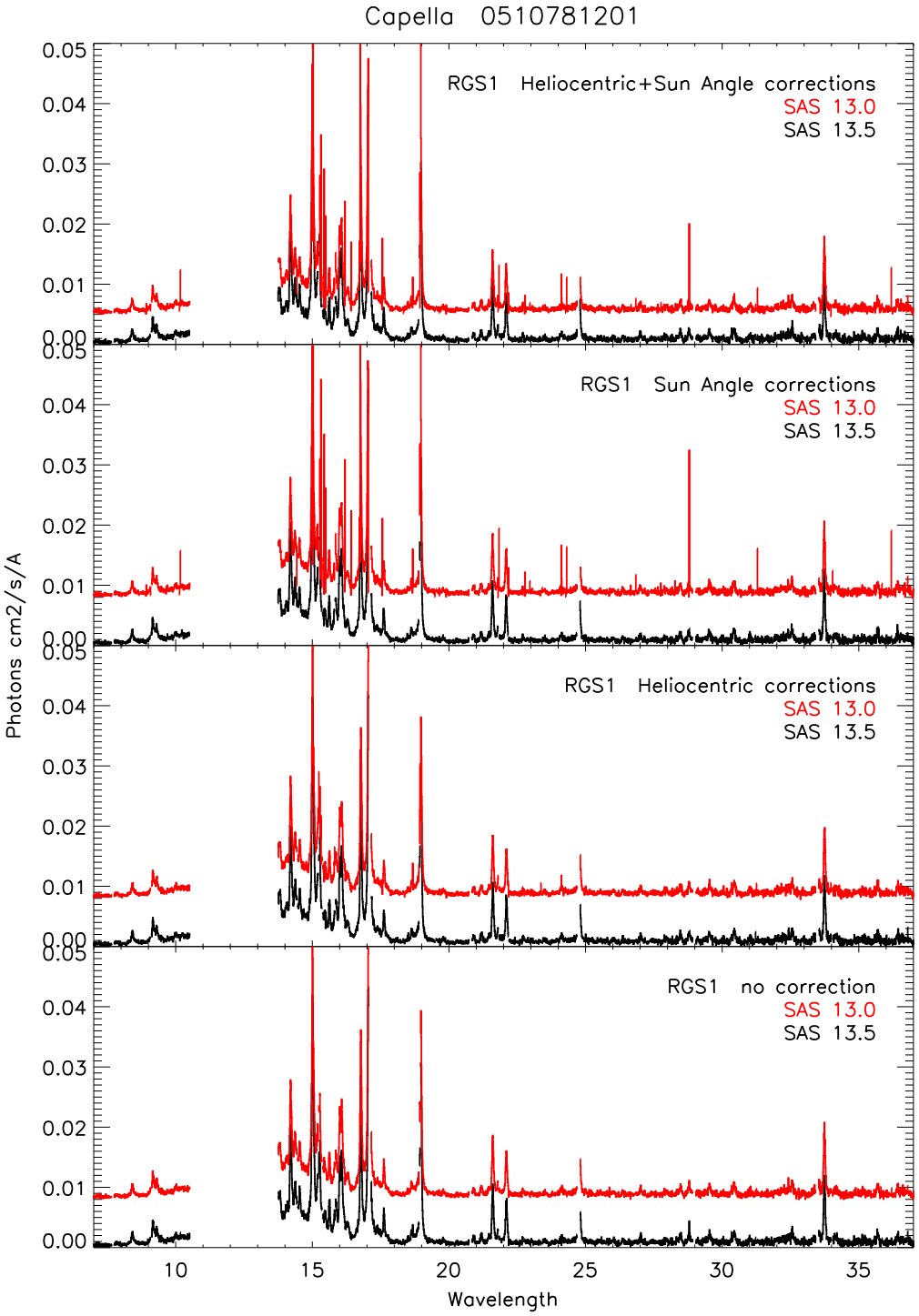

Figure 30: Comparison of the RGS1 fluxed spectra of one observation of Capella processed with SAS 13.0 and SAS 13.5 using different corrections to the wavelength scale. The spectra processed with SAS 13.0 corrected for Sun Angle dependence show prominent outliers at ≈ 10, 22, 24, 29 and 32 Å. These features do not appear when the spectra are obtained with SAS 13.5.

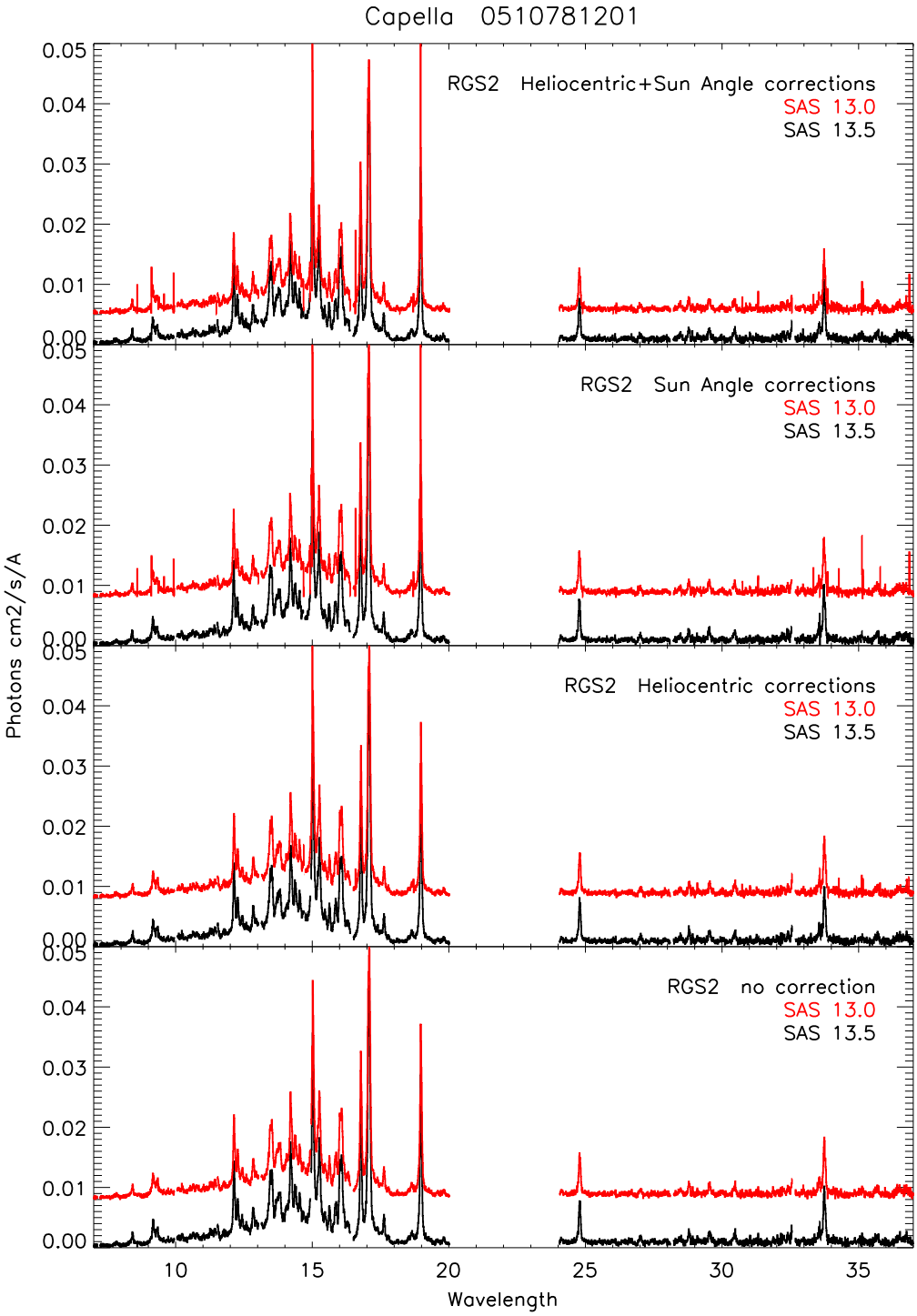

Figure 31: Same as the previous figure, but for RGS2. Note the outliers at 10, 35 and 36 Å in the spectra processed with SAS 13.0.

5 Conclusions

The main conclusion of the SAS 13.0 and 13.5 SV exercises can be summarized as follows:

- both versions can reduce data taken with all the EPIC, OM, and RGS scientific modes,
- event list produced with the `chain`s, the `proc`s, and with the PPS systems based on those SAS versions, albeit not identical, yield scientifically indistinguishable results,
- the flux cross-calibration among all X-ray cameras has improved at soft energies through the implementation of the EPIC-MOS contamination correction,
- introduction of a new algorithm to calculate the contribution of each pixel to the radial profile has recovered the nominal ±2% accuracy of the ELLBETA PSF calibration,
- introduction of a model for contamination of the MOS cameras (primarily MOS2) explains very well the time dependency of the response,
- SASv13.0 and SASv13.5 include calibrated corrections of X-ray loading effects for imaging and timing modes respectively,
- the wavelength scale uncertainty of RGS data has been reduced to few mÅthanks to the introduction of heliocentric and sun angle corrections in SASv13.0. A fix in SASv13.5 helped to avoid the eventual appearance of outliers in the RGS spectra after these corrections,
- a new task is available and validated (`multixmmselect`), which allows users to combine an arbitrary number of event files for selection of source and background regions followed by individual component spectra and / or light curves plus response matrices derivation, and their eventual merging,
- a new task for pile-up estimation and correction on PN data based on a novel method has been included in SASv13.

6 Acknowledgements

We are thankful to Michael Freyberg (MPE), J. de Plaa and C. de Vries (SRON) for their valuable comments and help during the validation processes.

References

Gabriel et al. 2001, XMM-SOC-USR-TN-0004
Gabriel et al. 2002, XMM-SOC-USR-TN-0009
Gabriel at al. 2008, XMM-SOC-USR-TN-0017
Guainazzi et al. 2012, XMM-CCF-REL-281
Read et al. 2011, A&A, 534, 34
Sánchez-Fernández, C., Santos-Lleó, M., in 't Zand, J. J. M., et al. 2006, AN 327, 1004
Shu, X. W., Yaqoob, T., Murphy, K. D., et al. 2010, ApJ 713, 1256
Tsujimoto et al. 2011, A&A, 525. A25
't Zand, J. J. M., Markwardt, C. B., Bazzano, A., et al. 2002, A&A 390, 597